PERGAMON

International Journal of Solids and Structures 38 (2001) 519–546

INTERNATIONAL JOURNAL OF SOLIDS and STRUCTURES

www.elsevier.com/locate/ijsolstr

On the formulation of anisotropic elastic degradation. II. Generalized pseudo-Rankine model for tensile damage

Ignacio Carol [a,c,*], Egidio Rizzi [b], Kaspar Willam [c]

[a] *ETSECCPB, Technical University of Catalonia, Jordi Girona 1-3, Edif. D2, E-08034 Barcelona, Spain*
[b] *Politecnico di Bari, Facoltà di Ingegneria di Taranto, Dip. Ingegneria Strutturale, I-70125 Bari, Italy*
[c] *Department of CEAE, University of Colorado, Boulder, CO 80309, USA*

Received 15 January 1999

Abstract

In the companion 'Part I' article, the theoretical aspects of anisotropic damage based on second-order tensors were discussed, and the concept of pseudo-logarithmic rate of damage was introduced. The thermodynamic forces conjugate to this damage rate exhibit physical meaning, which greatly simplifies the task of defining loading surfaces and evolution laws. In this second part, a formulation for anisotropic tensile damage which takes advantage of those concepts is developed and verified: the 'generalized pseudo-Rankine' model. Depending on the value of a single parameter, the loading surface in pseudo-log space may assume shapes which vary gradually between a π-plane and a Rankine-type criterion. This corresponds to a transition from a purely isotropic to a highly anisotropic tensile degradation model. In spite of the relative complexity of anisotropy, one of the important advantages of the model is that closed-form solutions are possible for a number of simple loading cases. The first one developed is uniaxial tension, which makes it possible to interpret the remaining two material parameters in terms of the tensile strength σ_t and fracture energy per unit volume g_f. Adding the two isotropic elastic constants, this makes a total of only five material parameters. Additional closed-form solutions are developed for the simple loading cases of pure shear, pure distortion, and uniaxial tension after tensile loading–unloading in a perpendicular direction. The behavior of the new model under complex loading histories is illustrated with a numerical tension/shear test with a significant rotation of principal strains.

Keywords: Elastic degradation; Plasticity; Fracture; Constitutive modeling

1. Introduction

In the companion paper (Carol et al., 2000), (referred to as "Part I" in the sequel), the authors expanded their theoretical framework of elastic degradation and damage (Carol et al., 1994). A theory of anisotropic damage was presented based on a second-order tensor secant formulation and on the novel concept of pseudo-logarithmic rate of damage. By introducing this rate of damage, the corresponding conjugate forces

* Corresponding author. Fax: +34-93-401-7251.
E-mail address: ignacio.carol@upc.es (I. Carol).

0020-7683/01/$ - see front matter
PII: S0020-7683(00)00031-7

turn out to exhibit clear physical meaning in terms of effective stress and effective strains, which greatly facilitates the task of defining loading surfaces and evolution laws.

In this "Part II", these new theoretical concepts are exploited with the development of the *generalized pseudo-Rankine model*, which aims at the tensile behavior of concrete and other quasi-brittle materials.

The fundamental equations of the model, presented in Section 2, are developed in four steps: selection of the fundamental variables, definition of the loading surface, calculation of gradients and damage rules, and formulation of hardening/softening laws. Although no stiffness recovery is considered in this article, special provisions are made to distinguish between tension and compression for the generation of new damage. In the proposal, the model has only five parameters: the two initial elastic moduli E^0 and ν^0, plus three more. The first of them, b, determines the degree of anisotropy of the model, which is related to the shape of the loading surface. All this is also described in Section 2. The remaining two parameters are related to the uniaxial tension stress–strain diagram of the material.

The formulation has the advantage of permitting closed-form solutions for simple loading cases. In Section 3, such a type of solution is derived for the uniaxial tension case, which is very convenient for interpreting the two remaining model parameters in terms of the tensile strength σ_t and the fracture energy per unit volume g_f. In Section 4, additional closed-form solutions are presented, for pure shear and pure distortion, and for the dependency of the current tensile strength on a previous loading–unloading sequence in a perpendicular direction.

In Section 5, an example of complex loading is presented. In this numerical test, the model is subjected to tension/shear with significant rotation of the prescribed principal strain directions (Willam et al., 1987). Detailed numerical results are presented that unveil a rich anisotropic response with features similar to what is obtained with more complicated models. Finally, Section 6 concludes with a summary of the main features, advantages and results of the formulation presented.

2. Definition of the model

2.1. Conjugate force variables

In Part I, a second-order anisotropic damage formulation based on energy equivalence and evolution laws in terms of a pseudo-logarithmic damage tensor rate $\dot{L}_{ij}$, was developed. Recalling Section 5 of Part I, the dissipation rate was obtained as

$$\dot{d} = \left(-\mathscr{Y}_{ij}\right)\dot{L}_{ij} = \left(-\mathscr{Y}_{ij}\right)\mathscr{M}_{ij}\dot{\lambda} = \dot{\lambda}\sum_{k=1}^{3}\left(-\mathscr{Y}_{(k)}\right)\mathscr{M}_{(k)}, \tag{1a–c}$$

where $-\mathscr{Y}_{ij}$ is the thermodynamic force conjugate to $\dot{L}_{ij}$. The second equality is obtained by replacing the decomposition of the damage rate into a non-negative scalar multiplier and damage rule $\dot{L}_{ij} = \dot{\lambda}\mathscr{M}_{ij}$, and the third one by assuming that the damage rule is defined with same principal axes as the conjugate force. Assuming linear isotropic elasticity between effective stresses and effective strains, the conjugate force could be expressed in the simple convenient form,

$$-\mathscr{Y}_{ij} = \tfrac{1}{2}\sigma^{\mathrm{eff}}_{ik}\epsilon^{\mathrm{eff}}_{kj} \tag{2}$$

or, in principal values,

$$-\mathscr{Y}_{(k)} = \tfrac{1}{2}\sigma^{\mathrm{eff}}_{(k)}\epsilon^{\mathrm{eff}}_{(k)}, \quad k = 1,2,3. \tag{3}$$

This force is a fundamental variable as it defines the space in which we will establish the loading surface and the damage rule. As given by the previous equations, however, this force does not distinguish between

tension and compression, which is a fundamental aspect of the behavior of quasi-brittle materials. In the previous equation, $-\mathscr{Y}_{(k)}$ has the same value whether $\sigma^{\text{eff}}_{(k)}$ and $\epsilon^{\text{eff}}_{(k)}$ are both positive or both negative. Therefore, a loading function and a damage rule based on those variables exclusively will not be able to distinguish between tension and compression. If the objective of the model is to represent tensile damage, the damage rule has to be re-defined such that $\mathscr{M}_{(k)} > 0$ only for those principal directions subject to tension, while $\mathscr{M}_{(k)} = 0$ for those subject to compression.

Another difficulty with the definition in Eqs. (2) and (3) is that the negative values $-\mathscr{Y}_{(k)} < 0$ could be obtained when $\sigma^{\text{eff}}_{(k)} > 0$ and $\epsilon^{\text{eff}}_{(k)} < 0$, or vice versa. As isotropic linear elasticity has been assumed between effective stresses and effective strains, this could correspond for instance to cases with principal stresses of the same sign but values much higher in one direction than the other. In such a situation, the Poisson effect caused by the major stresses may be greater than the strain due to the minor stresses themselves, causing strains with a sign opposite to that of applied stresses. From Eq. (1a–c), it follows that negative dissipation may be obtained if the damage is allowed to develop in the direction of a negative $-\mathscr{Y}_{(k)}$. In order to avoid this, a restriction must be imposed that $\mathscr{M}_{(k)} = 0$, whenever $-\mathscr{Y}_{(k)} < 0$.

The sign of the principal conjugate forces $-\mathscr{Y}_{(k)}$ in various regions of the effective stress space may be conveniently represented in the 2-D domain $\sigma^{\text{eff}}_{(1)}, \sigma^{\text{eff}}_{(2)}$, taking $\sigma^{\text{eff}}_{(3)} = 0$ (for plane conditions, the usual convention that 3 is the out-of-plane principal component even if it might not be the lowest, is adopted throughout the article). The well-known linear elastic relations $\epsilon^{\text{eff}}_{(1)} = (\sigma^{\text{eff}}_{(1)} - \nu^0\sigma^{\text{eff}}_{(2)})/E_0$ and $\epsilon^{\text{eff}}_{(2)} = (\sigma^{\text{eff}}_{(2)} - \nu^0\sigma^{\text{eff}}_{(1)})/E_0$ may be introduced into Eq. (3), and the resulting $-\mathscr{Y}_{(1)}$ and $-\mathscr{Y}_{(2)}$ are depicted in Fig. 1(a) and (b), in the form of contour levels. In Fig. 1(a), the domain is divided in four regions separated by the y-axis and by the inclined straight line $\sigma^{\text{eff}}_{(1)} = \nu^0\sigma^{\text{eff}}_{(2)}$. In the two larger regions labeled 1 and 2, $-\mathscr{Y}_{(1)}$ is positive; in region 1 with positive $\sigma^{\text{eff}}_{(1)}$ and $\epsilon^{\text{eff}}_{(1)}$, and with negative values for both in region 2. In the other two narrow wedge regions labeled 3 and 4, stress and strain have opposite signs, with resulting negative values of the

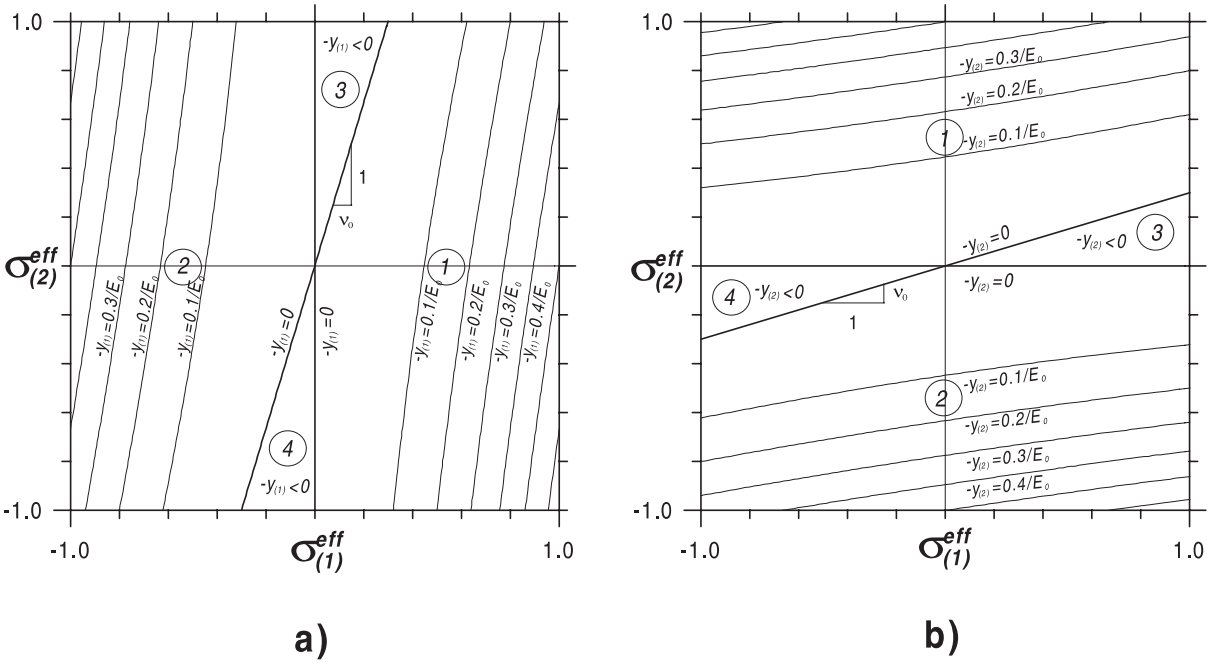

Fig. 1. 2D contour levels of the conjugate forces in the $\sigma^{\text{eff}}_{(1)}, \sigma^{\text{eff}}_{(2)}$ space for $\nu^0 = 0.3$: (a) $-\mathscr{Y}_{(1)}$, and (b) $-\mathscr{Y}_{(2)}$.

first component of the conjugate force. Similar contour levels and regions for $-\mathscr{Y}_{(2)}$ are represented in Fig. 1(b).

In order to handle previous difficulties and restrictions in a convenient way, the conjugate force may be redefined as follows:

$$\begin{aligned} -\hat{\mathscr{Y}}_{(1)} &= \tfrac{1}{2}\langle\sigma^{\mathrm{eff}}_{(1)}\rangle\langle\epsilon^{\mathrm{eff}}_{(1)}\rangle, \\ -\hat{\mathscr{Y}}_{(2)} &= \tfrac{1}{2}\langle\sigma^{\mathrm{eff}}_{(2)}\rangle\langle\epsilon^{\mathrm{eff}}_{(2)}\rangle, \\ -\hat{\mathscr{Y}}_{(3)} &= \tfrac{1}{2}\langle\sigma^{\mathrm{eff}}_{(3)}\rangle\langle\epsilon^{\mathrm{eff}}_{(3)}\rangle, \end{aligned} \tag{4a–c}$$

where the angle brackets are McAuley brackets with the usual meaning (i.e. $\langle x\rangle = x$ if $x > 0$ and $\langle x\rangle = 0$ otherwise). Note that this redefinition actually does not change the resulting dissipation as given by Eq. (1a–c), because in those regions where the value of one or more principal components of the original conjugate force are modified, the corresponding component(s) of the damage rule are required to be zero.

In order to ensure not only continuity but also smoothness across the boundaries of the regions implied by the modified forces, one additional restriction is placed on the damage rule. It is required to be perpendicular to the axis $-\hat{\mathscr{Y}}_{(1)}$ (i.e. vanishing component $\mathscr{M}_{(1)} = 0$) for states lying on the plane $-\hat{\mathscr{Y}}_{(2)}$, $-\hat{\mathscr{Y}}_{(3)}$, and similarly for the remaining two axes/planes. If the model is associated, this restriction translates into the geometrical requirement that, at its intersection with the coordinate planes $-\hat{\mathscr{Y}}_{(1)}$,$-\hat{\mathscr{Y}}_{(2)}$, or $-\hat{\mathscr{Y}}_{(2)}$, $-\hat{\mathscr{Y}}_{(3)}$, or $-\hat{\mathscr{Y}}_{(3)}$,$-\hat{\mathscr{Y}}_{(1)}$, the loading surface must be always perpendicular to those planes, as it will be satisfied by the specific loading function described in the next section.

After the previous definitions and assumptions, the following additional remarks are in order:

- The principal components of the modified force $-\hat{\mathscr{Y}}_{(1)}$,$-\hat{\mathscr{Y}}_{(2)}$,$-\hat{\mathscr{Y}}_{(3)}$ are intrinsically positive. As a consequence, the definition of the loading surface will be restricted to the positive–positive–positive octant of that space (this is in contrast with the original conjugate forces, which could take negative principal values and the surface had to be defined also outside that octant).
- With the modified forces (4), compressive damage cannot be represented. This type of damage is left out of the scope of this article.
- Note the symmetric role of stress and strain in the modified forces. The absence of a preferential role of stress or strain has been a characteristic of the general framework of elastic degradation and damage proposed by the authors (Carol et al., 1994), and of the specification of the theory to second-order damage and pseudo-logarithmic rate described in Part I. It is remarkable that this property can be also maintained in Eq. (4a–c).

2.2. Loading surface in the conjugate force space

The loading function is defined according to the general structure proposed in Section 6 of Part I, i.e.

$$F = f(-\hat{\mathscr{Y}}) - r(\text{history}). \tag{5}$$

For f, the algebraic expression proposed by Chaboche et al. (1994) is adopted

$$f(-\hat{\mathscr{Y}}) = \left(\left(-\hat{\mathscr{Y}}_{(1)}\right)^{b+1} + \left(-\hat{\mathscr{Y}}_{(2)}\right)^{b+1} + \left(-\hat{\mathscr{Y}}_{(3)}\right)^{b+1} \right)^{1/(b+1)}, \tag{6}$$

where b is a positive constant parameter $b \geqslant 0$, which determines the shape of the surface between the two limit cases of $b \to \infty$ and $b \to 0$.

In the limit case of $b \to \infty$, the surface $F = 0$ approaches a Rankine-type criterion in the space of modified conjugate forces $-\hat{\mathscr{Y}}$, which we call the *pseudo-Rankine* damage surface. In the sub-region $-\hat{\mathscr{Y}}_{(1)} \geqslant -\hat{\mathscr{Y}}_{(2)} \geqslant -\hat{\mathscr{Y}}_{(3)} \geqslant 0$, f may be rewritten as

$$f = -\hat{\mathscr{Y}}_{(1)}. \tag{7}$$

Note that, assuming that principal values are always ordered $-\hat{\mathscr{Y}}_{(1)} \geqslant -\hat{\mathscr{Y}}_{(2)} \geqslant -\hat{\mathscr{Y}}_{(3)}$, the surface needs only to be defined in that sixth of the positive–positive–positive octant, and for the rest of the domain, it is generated by symmetry.

In the opposite case with $b \to 0$, the loading surface approaches a deviatoric plane in $-\hat{\mathscr{Y}}$ space with an expression

$$f = -\hat{\mathscr{Y}}_{(1)} - \hat{\mathscr{Y}}_{(2)} - \hat{\mathscr{Y}}_{(3)}. \tag{8}$$

For intermediate values of b, a continuous transition of surfaces is obtained between the two limit cases. For instance, for $b = 1$, the surface becomes a spherical sector. All this is represented in Fig. 2(a) and (b), which depict a 3-D view of the surface for $b = 5$, and the 2-D cross-sections of the surface with the plane $-\hat{\mathscr{Y}}_{(3)} = 0$, for various values of b. Note that, for any $b > 0$, this surface is always perpendicular to the coordinate planes at their intersection, and it provides smooth transition (no corners) at the symmetry planes $-\hat{\mathscr{Y}}_{(1)} = -\hat{\mathscr{Y}}_{(2)}$, $-\hat{\mathscr{Y}}_{(2)} = -\hat{\mathscr{Y}}_{(3)}$ and $-\hat{\mathscr{Y}}_{(3)} = -\hat{\mathscr{Y}}_{(1)}$, which is important for numerical implementation.

The limit case with $b = 0$ is a special case which requires additional clarification. As the loading surface becomes a deviatoric plane, the requirement of orthogonality to the coordinate axes/planes cannot be maintained without generating a discontinuity of the gradients at the intersections. At the same time, it would seem natural that in this case, the model collapses into isotropic damage, and this corresponds to a damage rule always parallel to the p-axis ($\mathscr{M}_{(1)} = \mathscr{M}_{(2)} = \mathscr{M}_{(3)}$), which is incompatible with the assumption that individual components of $\mathscr{M}$ should vanish in specific situations (Section 2.1). As the consequence, for $b = 0$, all those conditions are relaxed and the model is simply defined separately as the isotropic damage model that would be 'closest' to the general anisotropic formulation. This definition is given by previous loading function (8), and by the normals always parallel to the p-axis, as specified in Section 2.3. Note that as Eq. (8) is written in terms of the modified forces (4), which include only tensile contributions, the isotropic model for $b = 0$ in general is not equivalent to the classical "$(1 - D)$" associated damage model, but to a non-associated 'tension-driven' version of it; only if all three principal components of effective stress

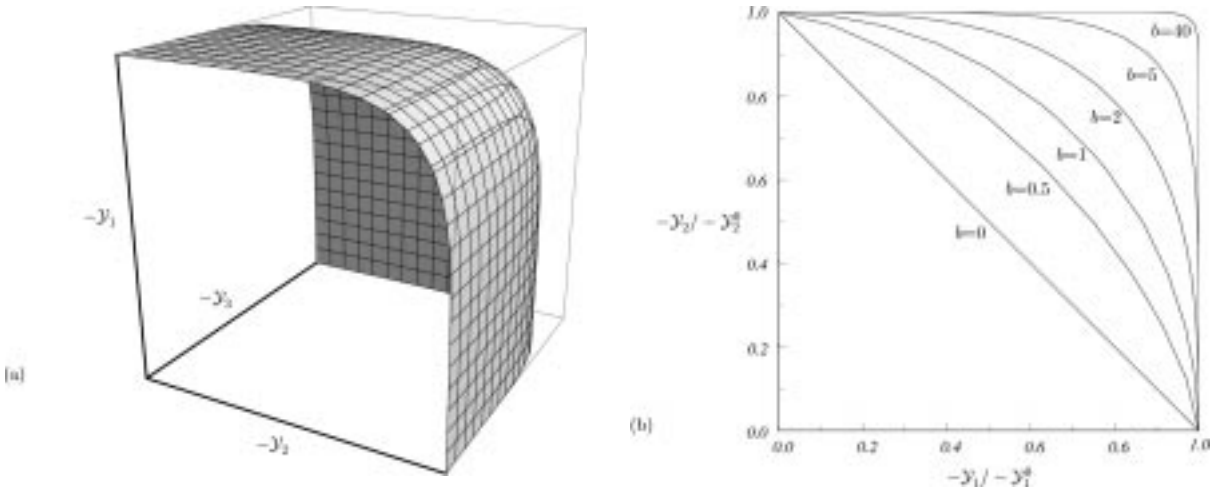

Fig. 2. The loading surface for the generalized pseudo-Rankine model: (a) 3D view for $b = 5$, and (b) 2D cross-section for $-\mathscr{Y}_3 = 0$, for $b = 0,\ 0.5,\ 1,\ 2,\ 5$ and 40.

and effective strain are positive, the modified force then becomes equal to the original, and the model equals the classical associated formulation.

2.3. Shape of the surface in stress space

The loading surface just defined may also be represented in the principal stress space. In general, this representation is only possible in terms of the effective stresses. However, for initial conditions with no damage, effective stresses coincide with nominal stresses and the same diagram will also represent the initial loading surface in nominal stress space.

Considering the 2-D case again with $\sigma^{\text{eff}}_{(3)} = 0$ for the sake of representation, the principal effective strains in Eq. (4a–c) may be replaced by the linear elastic relations $\epsilon^{\text{eff}}_{(1)} = (\sigma^{\text{eff}}_{(1)} - \nu^0\sigma^{\text{eff}}_{(2)})/E_0$ and $\epsilon^{\text{eff}}_{(2)} = (\sigma^{\text{eff}}_{(2)} - \nu^0\sigma^{\text{eff}}_{(1)})/E_0$, and the resulting forces may be substituted into the loading function (5), (6). According to the signs of effective stresses and effective strains discussed in Fig. 1, the McAuley brackets determine three regions with different algebraic expressions:

$$\begin{aligned}
&\text{Region 1}: \quad \sigma^{\text{eff}}_{(1)} > \nu^0\sigma^{\text{eff}}_{(2)}, \quad \sigma^{\text{eff}}_{(2)} > \nu^0\sigma^{\text{eff}}_{(1)} \rightarrow f = \frac{1}{2E^0}\left[\left(\sigma^{\text{eff}}_{(1)}\left(\sigma^{\text{eff}}_{(1)} - \nu^0\sigma^{\text{eff}}_{(2)}\right)\right)^{b+1}\right. \\
&\qquad\qquad \left. + \left(\sigma^{\text{eff}}_{(2)}\left(\sigma^{\text{eff}}_{(2)} - \nu^0\sigma^{\text{eff}}_{(1)}\right)\right)^{b+1}\right]^{1/(b+1)}, \\
&\text{Region 2}: \quad \sigma^{\text{eff}}_{(1)} \leqslant \nu^0\sigma^{\text{eff}}_{(2)}, \quad \sigma^{\text{eff}}_{(2)} > 0 \rightarrow f = \frac{1}{2E^0}\sigma^{\text{eff}}_{(2)}\left(\sigma^{\text{eff}}_{(2)} - \nu^0\sigma^{\text{eff}}_{(1)}\right), \\
&\text{Region 3}: \quad \sigma^{\text{eff}}_{(2)} \leqslant \nu^0\sigma^{\text{eff}}_{(1)}, \quad \sigma^{\text{eff}}_{(1)} > 0 \rightarrow f = \frac{1}{2E^0}\sigma^{\text{eff}}_{(1)}\left(\sigma^{\text{eff}}_{(1)} - \nu^0\sigma^{\text{eff}}_{(2)}\right).
\end{aligned} \tag{9a–c}$$

The resulting loading surface $F = 0$ for various values of parameter b is represented in Fig. 3, with a general view in Fig. 3(a) and close-up of the tension–tension sector in Fig. 3(b). In the figure, Region 1 corresponds to the wedge area between the straight lines $\sigma^{\text{eff}}_{(1)} = \nu^0\sigma^{\text{eff}}_{(2)}$ and $\sigma^{\text{eff}}_{(2)} = \nu^0\sigma^{\text{eff}}_{(1)}$ in the tension–tension sector (Fig. 3(b)), whereas Regions 2 and 3 extend to the left and right of that wedge.

Overall, the shape of the surface agrees well with the tensile-dominated parts of the standard biaxial failure diagram for concrete (Kupfer and Gerstle, 1973). In Regions 2 and 3, the surface is not affected by parameter b, which in contrast has significant influence in the tension–tension corner of Region 1. Continuity of derivatives is maintained between regions, except for the isotropic case $b = 0$, which did not exhibit such continuity in the conjugate force space (not perpendicular at the intersections with the coordinate planes). Higher values of b produce a higher curvature of the surface in the tensile–tensile sector, which, in the limit case of the 'pure' pseudo-Rankine model ($b \rightarrow \infty$), becomes a mere continuation of the curves in Regions 2 and 3, meeting at a sharp corner at the equi-tension line $\sigma^{\text{eff}}_{(1)} = \sigma^{\text{eff}}_{(2)}$.

2.4. Damage rule

In the anisotropic case $b > 0$, the model is assumed to be associated. As the loading function is defined in terms of the principal values of the conjugate force, the damage rule may be expressed as

$$\mathscr{M}_{ij} = \mathscr{N}_{ij} = \frac{\partial f}{\partial(-\hat{\mathscr{Y}}_{ij})} = \sum_{k=1}^{3} \mathscr{N}_{(k)} t_i^{(k)} t_j^{(k)}, \quad \mathscr{N}_{(k)} = \frac{\partial F}{\partial(-\hat{\mathscr{Y}}_{(k)})}, \tag{10a–d}$$

where the principal gradients $\mathscr{N}_{(k)}$ may be directly obtained from Eq. (6), and $t_i^{(k)}$ are the components of the unit vectors in the directions of the major principal effective stress and strain, according to the spectral decompositions:

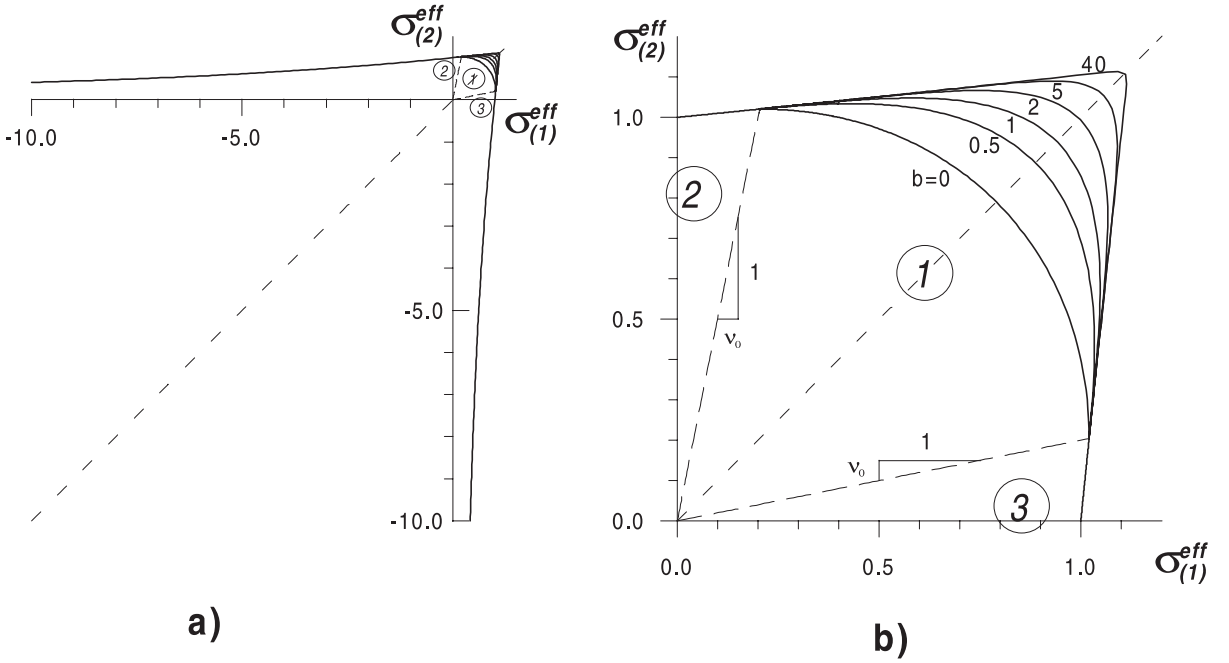

Fig. 3. 2D representation of the loading surface in effective stress space.

$$\sigma_{ij}^{\text{eff}} = \sum_{k=1}^{3} \sigma_{(k)}^{\text{eff}} t_i^{(k)} t_j^{(k)}, \quad \epsilon_{ij}^{\text{eff}} = \sum_{k=1}^{3} \epsilon_{(k)}^{\text{eff}} t_i^{(k)} t_j^{(k)}, \quad -\hat{\mathscr{Y}}_{ij} = \sum_{k=1}^{3} -\hat{\mathscr{Y}}_{(k)} t_i^{(k)} t_j^{(k)}. \tag{11a–c}$$

For the case $b = 0$, the isotropic damage rule is assumed independently of F, as already explained in the previous section. This leads to the following expressions:

$$\text{if } b > 0, \quad \mathscr{M}_{(k)} = \frac{\left(-\hat{\mathscr{Y}}_{(k)}\right)^b}{\left(\left(-\hat{\mathscr{Y}}_{(1)}\right)^{(b+1)} + \left(-\hat{\mathscr{Y}}_{(2)}\right)^{(b+1)} + \left(-\hat{\mathscr{Y}}_{(3)}\right)^{(b+1)}\right)^{b/(b+1)}},$$

$$\text{if } b = 0, \quad \mathscr{M}_{(1)} = \mathscr{M}_{(2)} = \mathscr{M}_{(3)} = 1 \quad \left(\text{i.e. } \mathscr{M}_{ij} = \delta_{ij}\right). \tag{12a, b}$$

Note that, for $b \to \infty$ (pseudo-Rankine), Eq. (12a,b) reduces to

$$\mathscr{M}_{(1)} = 1, \quad \mathscr{M}_{(2)} = \mathscr{M}_{(3)} = 0 \quad \left(\text{i.e. } \mathscr{M}_{ij} = t_i^{(1)} t_j^{(1)}\right). \tag{13a–c}$$

With $\mathscr{N}_{ij}$ and $\mathscr{M}_{ij}$ defined, and considering a generic resistance function r(hist), the gradients in compliance and stress space N_{ijkl} and n_{ij}, the corresponding flow rules M_{ijkl} and m_{ij} and the hardening/softening moduli H and $\bar{H}$ may be determined using Eqs. (77b,c), (78b,c), (79) and (80) from Part I, in which the partial derivative $\partial C_{ijkl}/\partial L_{rs}$ is given by Eq. (69(b)) and the partial derivative $\partial(-\mathscr{Y}_{pq})/\partial L_{rs}$ is given in Appendix 3, of Part I as well.

For a general value of b, analytical substitution of those partial derivatives leads to lengthy equations that are not strictly necessary for the implementation of the model (substitutions may be done directly with numerical values). However, in the limit cases $b = 0$ and $b \to \infty$, it is possible to obtain simplified analytical expressions which offer further insight. For $b = 0$ (isotropic damage), expressions similar to Eqs. (29)–(35)

of Part I are recovered. In the other limit $b \to \infty$ (pseudo-Rankine), laborious substitutions and simplifications lead to the following expressions:

$$M_{ijkl} = N_{ijkl} = \frac{-\nu^0}{2E^0}\left[\phi_{ij} w_k^{(t1)} w_l^{(t1)} + \phi_{kl} w_i^{(t1)} w_j^{(t1)}\right] + \frac{1+\nu^0}{4E^0}\left[\phi_{ik} w_j^{(t1)} w_l^{(t1)} + \phi_{il} w_j^{(t1)} w_k^{(t1)} + \phi_{jk} w_i^{(t1)} w_l^{(t1)} + \phi_{jl} w_i^{(t1)} w_k^{(t1)}\right], \tag{14a, b}$$

$$m_{ij} = n_{ij} = \frac{1}{2}\left[-\frac{\nu^0}{E^0}\sigma_{(1)}^{\text{eff}}\phi_{ij} + \left(\frac{1+\nu^0}{E^0}\sigma_{(1)}^{\text{eff}} + \epsilon_{(1)}^{\text{eff}}\right) w_i^{(t1)} w_j^{(t1)}\right], \tag{15a, b}$$

$$-\bar{m}_{ij} = \bar{n}_{ij} = E_{ijkl} n_{kl} = \frac{1}{2}\left[\Lambda^0 \epsilon_{(1)}^{\text{eff}} \bar{\phi}_{ij} + \left(2G^0 \epsilon_{(1)}^{\text{eff}} + \sigma_{(1)}^{\text{eff}}\right) \bar{w}_i^{(t1)} \bar{w}_j^{(t1)}\right], \tag{16a, b}$$

$$H = \frac{\partial r}{\partial \lambda} - \frac{1}{4}\left[\sigma_{(1)}^{\text{eff}} \epsilon_{(1)}^{\text{eff}} + \frac{1}{E^0}\left(\sigma_{(1)}^{\text{eff}}\right)^2\right],$$
$$\bar{H} = \frac{\partial r}{\partial \lambda} + \frac{1}{4}\left[\sigma_{(1)}^{\text{eff}} \epsilon_{(1)}^{\text{eff}} + \left(\Lambda^0 + 2G^0\right)\left(\epsilon_{(1)}^{\text{eff}}\right)^2\right], \tag{17a, b}$$

where, for convenience, $w_i^{(t1)}$ and $\bar{w}_i^{(t1)}$ denote the "vector projections" of w_{ij} and $\bar{w}_{ij}$ on the first principal effective direction $t_j^{(1)}$:

$$w_i^{(t1)} = w_{ij} t_j^{(1)}, \qquad \bar{w}_i^{(t1)} = \bar{w}_{ij} t_j^{(1)}. \tag{18a, b}$$

2.5. Hardening/softening laws

The remaining aspect is to establish the resistance function r, which accounts for the previous damage history. As history is represented by the damage variables, it seems natural to assume that r depends on those variables. The simplest damage measure that may be considered in the context of the present theory seems to be the scalar quantity given by the first invariant of the pseudo-log damage tensor, i.e. $L = L_{kk}/3$. As explained in Appendix 1 of Part I, L coincides with the volumetric part of the "true" log damage:

$$L = \tfrac{1}{3}\left(\ln \phi_{(1)}^2 + \ln \phi_{(2)}^2 + \ln \phi_{(3)}^2\right) = \tfrac{2}{3}\ln(\phi_{(1)}\phi_{(2)}\phi_{(3)}). \tag{19a, b}$$

Aiming at the softening behavior due to tensile damage, the function proposed for $r(L)$ is a simple two-parameter exponential decay

$$r(\text{hist}) = r_0 \mathrm{e}^{-3kL}, \tag{20}$$

where $r_0 = \sigma_{\text{t}}^2/2E^0$ is the elastic energy at peak of the uniaxial tension test, and k is defined in terms of the Mode I fracture energy per unit volume g_{f} as follows: if $b = 0$, $k = r_0/3g_{\text{f}}$, while if $b > 0$, $k = r_0/g_{\text{f}}$ (note that g_{f} is defined as the area under the complete uniaxial stress–strain curve; Fig. 4). These relations will be justified in the following section after obtaining the closed-form solution for uniaxial tension. It is emphasized that the entire damage model has only 5 parameters: the two isotropic elastic moduli E^0, ν^0, the tensile strength σ_{t} and fracture energy density g_{f}, and the shape parameter b linked to the degree of anisotropy.

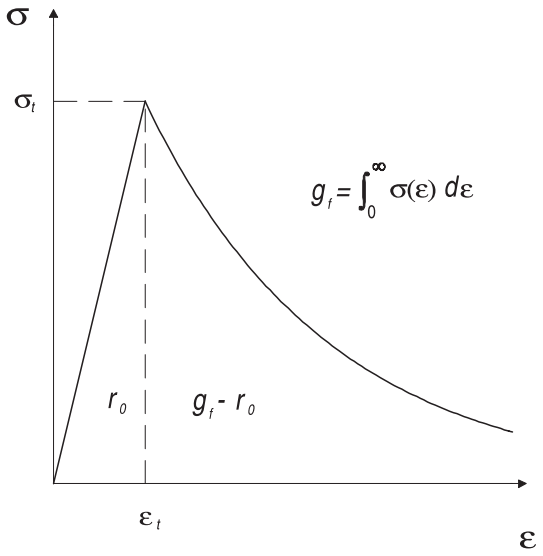

Fig. 4. The uniaxial tension stress–strain curve with representation of energies r_0 and g_f.

3. Closed-form solution in uniaxial tension

To better understand the behavior of the model and the physical meaning of r_0 and k, the loading case of uniaxial tension along axis x is now analyzed. This means that $\sigma_{(1)} = \sigma_{xx} \geqslant 0$, whereas all other $\sigma_{(i)}$ and $\sigma_{ij} \equiv 0$.

A crucial property in this derivation refers to the evolution of damage, for which two cases have to be distinguished:

(*a*) *Case* $b > 0$: The principal directions of damage remain fixed and the only component of damage that evolves is the principal value along the loading axis, i.e. $\phi_{(1)} = \phi_{xx}$, $\phi_{(2)} = \phi_{(3)} \equiv 1$. Also, the effective strains and stresses share the same principal axes and their largest eigenvalues are those along x, i.e. $\sigma^{\text{eff}}_{(1)} = \sigma^{\text{eff}}_{xx}$ and $\epsilon^{\text{eff}}_{(1)} = \epsilon^{\text{eff}}_{xx}$. With the generalized Rankine-type surface (and the associated damage rule), this is readily proven because the surface maintains orthogonality to the coordinate planes for $b > 0$. Initially, effective and nominal quantities coincide and the only non-zero principal effective stress is along the x-axis, and the same holds for the conjugate forces. Therefore, the damage rule (10) also has only one non-zero eigenvalue along the same axis, and this is the only term modified in ϕ_{ij} (or any of the alternative damage tensors). For subsequent loading, the situation remains the same because even with damage varying along x-axis, effective stress components (and therefore conjugate forces) remain zero along y and z. Consequently, we always have $\phi_{(2)} = \phi_{(3)} \equiv 1$.

(*b*) *Case* $b = 0$: Here, the damage rule is always the identity tensor (12b), and therefore, ϕ_{ij} remains spherical. Consequently, we have $\phi_{(2)} = \phi_{(3)} \equiv \phi_{(1)}$.

In both cases, the following simple relations apply:

$$\sigma^{\text{eff}}_{(1)} = \sigma_{(1)}\phi_{(1)}, \qquad \epsilon^{\text{eff}}_{(1)} = \frac{\epsilon_{(1)}}{\phi_{(1)}}. \tag{21a, b}$$

These equations may be directly substituted into Eq. (3), and the $\phi_{(1)}$ factors cancel out, leading to the following expression of the loading function (6)

$$F = \tfrac{1}{2}\sigma_{(1)}\epsilon_{(1)} - r. \tag{22}$$

In other terms, in this case, F may be directly expressed in terms of nominal stress and strain along the loading axis.

Upon application of the uniaxial tensile load, the model initially responds with linear elastic behavior until the loading surface $F = 0$ is reached at a contact point. Since the softening starts right from the beginning of inelastic behavior (20), this point corresponds to the peak of the uniaxial stress–strain diagram in tension, with stress and strains denoted as σ_t and ϵ_t. As this is still a point of the initial elastic response, these values satisfy $\sigma_t = E^0\epsilon_t$. At the same time, this is the first point at which $F = 0$, and therefore we may identify the initial value $r = r_0$ as the elastic energy at the peak

$$r_0 = \frac{1}{2}\sigma_t\epsilon_t = \frac{1}{2}\frac{\sigma_t^2}{E^0} = \frac{1}{2}E^0\epsilon_t^2. \tag{23a–c}$$

Upon persistent loading, the condition $F = 0$ is maintained. From this condition, we obtain the meaning of r as the current (secant) elastic energy, and extract a simple relation for stress

$$r = \frac{1}{2}\sigma_{(1)}\epsilon_{(1)}, \qquad \sigma_{(1)} = \frac{2r}{\epsilon_{(1)}}. \tag{24a, b}$$

Application of the general elastic stress–strain relations with the secant compliance (Eq. (65) of Part I) to this loading case, yields

$$\epsilon_{(1)} = \frac{\phi_{(1)}^2}{E^0}\sigma_{(1)}. \tag{25}$$

The stress may now be eliminated between this and the second of the previous equations; r may be substituted from the exponential law (20), and L replaced by its expression in terms of $\phi_{(1)}$ which, from Eq. (19a,b), is $L = \ln \phi_{(1)}^{2/3}$ if $b > 0$, or $L = \ln \phi_{(1)}^2$ if $b = 0$ (isotropic damage). The result is a relation between $\phi_{(1)}$ and $\epsilon_{(1)}$ which may in turn be backsubstituted into the previous expressions to obtain the following explicit equations for the post-peak descending branch of the uniaxial stress–strain diagram,

$$\text{if } b > 0, \quad \sigma_{(1)} = \sigma_t\left(\frac{\epsilon_{(1)}}{\epsilon_t}\right)^{-(1+k)/(1-k)}$$
$$\text{if } b = 0, \quad \sigma_{(1)} = \sigma_t\left(\frac{\epsilon_{(1)}}{\epsilon_t}\right)^{-(1+3k)/(1-3k)} \tag{26a, b}$$

For $k = 0$, the exponent is -1 in both cases, and we recover the hyperbolic decay that would correspond to Eq. (24a,b) with constant $r \equiv r_0$. For $k > 0$, we obtain sharper decays as k is higher, but note that k must be less than 1 (for $b > 0$) or 1/3 (for $b = 0$) to avoid loss of uniqueness. Those values would indeed correspond to vertical stress drop from the peak.

As already indicated, k may also be related to the Mode I fracture energy per unit volume g_f (Fig. 4), which has the advantage of a clearer physical meaning and provides a simple means of regularizing post-peak finite element computations. This is achieved by integrating the area under the stress–strain curve:

$$g_f = r_0 + \int_{\epsilon_t}^{\infty} \sigma_{(1)}\,\mathrm{d}\epsilon_{(1)}. \tag{27}$$

Substitution of (26) leads to the following simple relations between parameters:

$$\text{if } b>0, \quad k=\frac{r_0}{g_f},$$
$$\text{if } b=0, \quad k=\frac{r_0}{3g_f}. \tag{28a, b}$$

Note that the previous restriction on the values of k, translates (in both cases $b=0$ and $b>0$) into the condition that $g_f > r_0$, which corresponds to avoiding snap back in the uniaxial stress–strain relation.

Backsubstitution of k into the previous equations leads to the following expressions for r

$$\text{if } b>0, \quad r=r_0 e^{-3(r_0/g_f)L},$$
$$\text{if } b=0, \quad r=r_0 e^{-(r_0/g_f)L}. \tag{29a, b}$$

Most of the remaining unknowns of the problem have common expressions for $b>0$ and $b=0$:

$$\sigma_{(1)}=\sigma_t\left(\frac{\epsilon_{(1)}}{\epsilon_t}\right)^{-(g_f+r_0)/(g_f-r_0)}, \quad E=E^0\left(\frac{\epsilon_{(1)}}{\epsilon_t}\right)^{-2g_f/(g_f-r_0)}, \quad \phi_{(1)}=\left(\frac{\epsilon_{(1)}}{\epsilon_t}\right)^{g_f/(g_f-r_0)}, \tag{30a–c}$$

$$\sigma^{\text{eff}}_{(1)}=\sigma_t\left(\frac{\epsilon_{(1)}}{\epsilon_t}\right)^{-r_0/(g_f-r_0)}, \quad \epsilon^{\text{eff}}_{(1)}=\epsilon_t\left(\frac{\epsilon_{(1)}}{\epsilon_t}\right)^{-r_0/(g_f-r_0)}, \quad \epsilon^{\text{eff}}_{(2)}=\epsilon^{\text{eff}}_{(3)}=-\nu^0\epsilon^{\text{eff}}_{(1)} \tag{31a–c}$$

except the lateral nominal strains, which are

$$\text{if } b>0, \quad \epsilon_{(2)}=\epsilon_{(3)}=\epsilon^{\text{eff}}_{(2)}=\epsilon^{\text{eff}}_{(3)}=-\nu^0\epsilon_t\left(\frac{\epsilon_{(1)}}{\epsilon_t}\right)^{-r_0/(g_f-r_0)},$$
$$\text{if } b=0, \quad \epsilon_{(2)}=\epsilon_{(3)}=\phi_{(1)}\epsilon^{\text{eff}}_{(2)}=-\nu^0\epsilon_{(1)}. \tag{32a–c}$$

These solutions, for all variables except for the lateral nominal strains, are illustrated in Fig. 5 for the fixed parameter values $E^0=10^7$ kPa, $\nu^0=0.2$, $\sigma_t=10^4$ kPa, and changing values of g_f. In the first plot, the evolution of stress $\sigma_{xx}=\sigma_{(1)}$ is represented against the prescribed strain $\epsilon_{xx}=\epsilon_{(1)}$. It is apparent that, for $g_f=\infty$, the decay of σ_{xx} is the slowest, while for progressively lower finite values of g_f, softening is more pronounced. The effective stresses (second plot) exhibit a similar trend, but starting from a horizontal line for the case $g_f=\infty$, in which the stress decay is compensated in the same proportion by increase of the inverse integrity. For progressively lower finite values of g_f, effective stresses decrease more rapidly but always at a lower pace than their nominal counterparts. The third plot exhibits the evolution of the minor principal value of the integrity tensor, which in this case is $\bar{\phi}_{xx}=1/\phi_{xx}$. As it could be expected, decay is faster for lower values of g_f. In the fourth plot, the effective strains in the direction of loading and in the lateral directions, are illustrated against the prescribed axial strain. In the limiting case of $g_f=\infty$, effective strains remain constant after the peak, while for finite values of g_f, they decrease asymptotically to zero, faster as g_f decreases and approaches r_0. In the case $b>0$, the nominal lateral strains are the same as their effective counterparts. In the case $b=0$, the nominal lateral strains (not plotted) are simply proportional with constant Poisson's ratio ν^0 to the prescribed axial strain (corresponding to the "$(1-D)$" isotropic damage model, which modifies E^0 but not ν^0).

4. Other simple loading cases with a closed-form solution

Closed-form solutions similar to the one for uniaxial tension may also be obtained for other basic loading cases such as pure shear and pure distortion. Also, in these cases, the solution has to be derived separately for the case $b>0$ (anisotropic damage) and $b=0$ (isotropic damage). A closed-form solution is also obtained for the reduction of tensile strength due to previous tensile loading in a perpendicular direction.

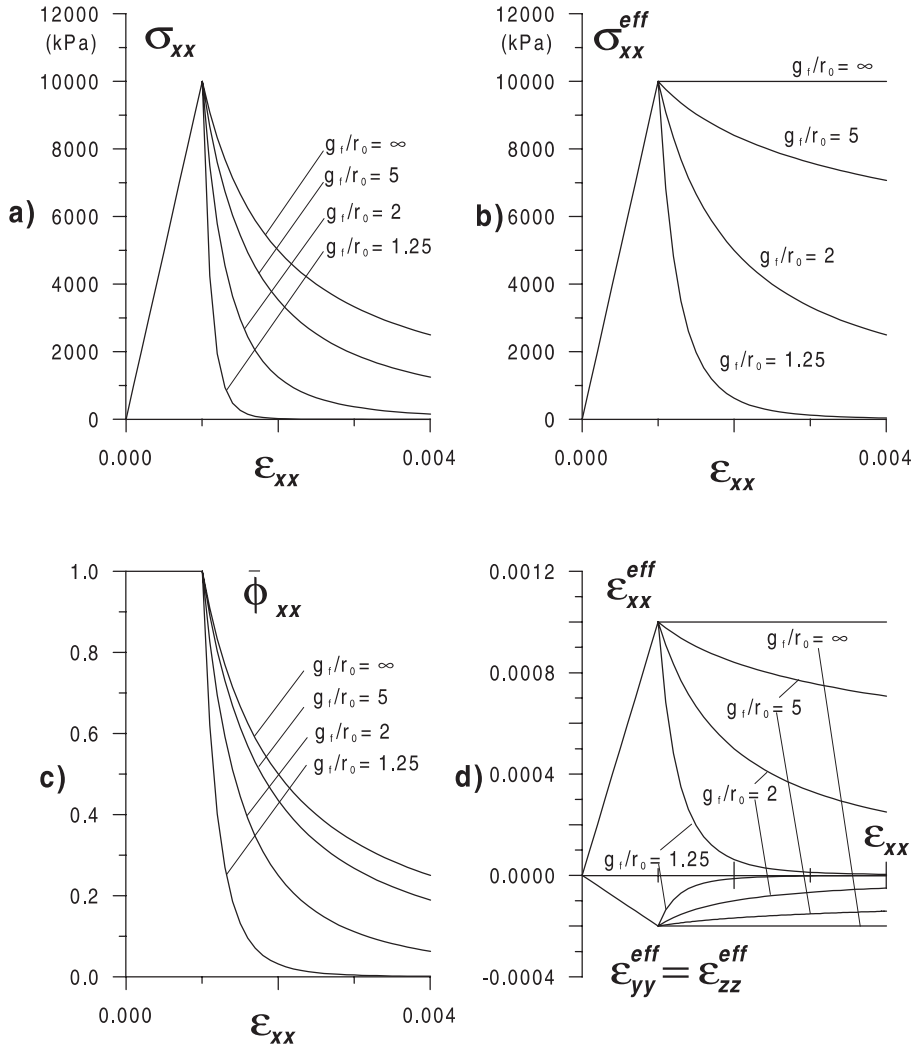

Fig. 5. The results obtained with generalized pseudo-Rankine model under uniaxial loading, for different values of parameter g_f. Evolution with respect to the prescribed uniaxial strain, of (a) stress, (b) effective stress, (c) integrity tensor, and (d) effective strains.

4.1. Pure shear for $b > 0$ (anisotropic damage)

The principal stresses that correspond to pure shear with prescribed intensity $\bar{\tau} > 0$ on planes at 45° are

$$\sigma_{(1)} = \bar{\tau}, \quad \sigma_{(2)} = -\bar{\tau}, \quad \sigma_{(3)} = 0. \tag{33a–c}$$

For increasing $\bar{\tau}$, this would represent a straight path at either −45° or 135° (tension/compression quadrants) in the biaxial stress space $\sigma_{(1)}$, $\sigma_{(2)}$. During the initial undamaged elastic regime, nominal stresses coincide with effective stresses, and the same representation would be valid on the effective stress space of Fig. 3. Similar arguments to the case of pure tension in previous section, lead to the conclusion that for $b > 0$, the only direction developing damage will be principal direction1, i.e. the one with the tensile stress. This means that $\phi_{(1)}$ is the only damage component growing from 1 to ∞ , while $\phi_{(2)} = \phi_{(3)} \equiv 1$ (note that

this is due to having written the loading function in terms of the modified conjugate forces (4) which distinguish tension from compression; otherwise, compressive direction 2 would also develop damage). This implies the following effective stresses (Eq. 60(b) of Part I):

$$\sigma^{\text{eff}}_{(1)} = \phi_{(1)}\bar{\tau}, \quad \sigma^{\text{eff}}_{(2)} = \sigma_{(2)} = -\bar{\tau}, \quad \sigma^{\text{eff}}_{(3)} = \sigma_{(3)} = 0. \tag{34a–c}$$

Using linear isotropic elasticity with parameters E^0, v^0, and the nominal-effective relations (Eq. (61), (62) of Part I), one can obtain the corresponding effective and nominal strains:

$$\epsilon^{\text{eff}}_{(1)} = \frac{\bar{\tau}}{E^0}(\phi_{(1)} + v^0), \quad \epsilon^{\text{eff}}_{(2)} = -\frac{\bar{\tau}}{E^0}(1 + v^0\phi_{(1)}), \quad \epsilon^{\text{eff}}_{(3)} = -v^0\frac{\bar{\tau}}{E^0}(\phi_{(1)} - 1), \tag{35a–c}$$

$$\epsilon_{(1)} = \frac{\bar{\tau}}{E^0}(\phi_{(1)} + v^0)\phi_{(1)}, \quad \epsilon_{(2)} = \epsilon^{\text{eff}}_{(2)}, \quad \epsilon_{(3)} = \epsilon^{\text{eff}}_{(3)}. \tag{36a–c}$$

In order to identify the strain γ conjugate to $\bar{\tau}$, the elastic energy is developed, leading to

$$u = \frac{1}{2}\sigma_{ij}\epsilon_{ij} = \frac{1}{2}\bar{\tau}\gamma, \quad \gamma = \epsilon_{(1)} - \epsilon_{(2)} = \frac{\bar{\tau}}{E_0}\left(1 + 2v^0\phi_{(1)} + \phi^2_{(1)}\right). \tag{37a–c}$$

In the elastic range, Eqs. (33a–c)–(37a–c) apply if we set $\phi_{(1)} = 1$. The loading condition is reached for the first time when $F = 0$, i.e.

$$F = \frac{1}{2}\sigma^{\text{eff}}_{(1)}\epsilon^{\text{eff}}_{(1)} - r_0 = \frac{\bar{\tau}^2}{2E^0}(1 + v^0) - r_0 = 0. \tag{38}$$

This value of $\bar{\tau}$ represents the elastic stress at the contact point with the loading surface for this type of loading (onset of damage), which we call τ_0. Taking advantage of previous relations (23), one may write

$$\tau_0 = \frac{\sigma_t}{\sqrt{1 + v^0}}. \tag{39}$$

After peak, the loading surface is enforced with the current value of r. For $b > 0$, this is given by Eq. (29a,b), in which $L = L_{kk}/3$ is the same as in uniaxial tension, i.e. $L = \ln \phi^{2/3}_{(1)}$. Replacing all these expressions, one obtains

$$F = \frac{1}{2}\sigma^{\text{eff}}_{(1)}\epsilon^{\text{eff}}_{(1)} - r = \frac{\bar{\tau}^2}{2E^0}(\phi_{(1)} + v^0)\phi_{(1)} - r_0\phi^{-2r_0/g_f}_{(1)} = 0. \tag{40}$$

The previous equation may be rewritten in the following convenient form:

$$\bar{\tau} = \tau_0\sqrt{\frac{1 + v^0}{\phi_{(1)} + v^0}}\,\phi^{-(1/2)-(r_0/g_f)}_{(1)}. \tag{41}$$

Replacing this relation into Eqs. (33a–c)–(36a–c), one may obtain all remaining stresses and strains, nominal and effective, in terms of the damage variable $\phi_{(1)}$. Finally, Eq. (41) may be replaced into the conjugate strain expression (37) to obtain

$$\gamma = \gamma_0\frac{1 + 2v^0\phi_{(1)} + \phi^2_{(1)}}{2(1 + v^0)}\sqrt{\frac{1 + v^0}{\phi_{(1)} + v^0}}\,\phi^{-(1/2)-(r_0/g_f)}_{(1)}, \tag{42}$$

where the peak strain is

$$\gamma_0 = 2\epsilon_t\sqrt{1 + v^0} = \frac{\tau_0}{G^0} \tag{43}$$

and G^0 is the initial shear modulus $G_0 = E_0/2(1 + v^0)$.

The form of Eqs. (41) and (42) is such that it is not easy to eliminate $\phi_{(1)}$ and obtain an explicit relation between $\bar{\tau}$ and γ. Nevertheless, one can use them as two parametric expressions in terms of $\phi_{(1)}$. By giving values between 1 and ∞ to this variable, pairs of values of $\bar{\tau}$ and γ may be generated and plotted in a diagram. This has been done in Fig. 6(a), for the parameter values $E^0 = 10^7$ kPa, $\nu^0 = 0.2$ and $\sigma_t = 10^4$ kPa (same as in the previous section), which leads to the values of $\tau_0 = 9129$ kPa and $\gamma_0 = 0.002191$. Various curves have been obtained for $g_f/r_0 = 1.001, 1.25, 2, 5$ and 100 (for practical purposes similar to ∞). Note that, also in this case, parameter b is irrelevant as long as $b > 0$.

Fig. 6(a) shows how brittle and unstable the post-peak response is for the pure shear loading case. Curves with snap-back are obtained for usual values of g_f/r_0 between 2 and 10. Actually, these results have to be interpreted carefully, because even those curves without snap-back would be unstable for the 'prescribed-stress' type of loading assumed (the curves can be plotted thanks to the parametric nature of the equations used, in which $\phi_{(1)}$ takes the role of always-increasing indirect control variable in the test). The precise value of g_f/r_0 for which snap-back disappears may be obtained from previous Eqs. (41) and (42). The slope of the shear response is given by the derivative of $\bar{\tau}$ with respect to γ, which can be expanded via chain rule

$$\frac{\partial\bar{\tau}}{\partial\gamma} = \frac{\partial\bar{\tau}}{\partial\phi_{(1)}}\frac{\partial\phi_{(1)}}{\partial\gamma} = \frac{\partial\bar{\tau}}{\partial\phi_{(1)}}\frac{1}{\partial\gamma/\partial\phi_{(1)}}. \tag{44}$$

In particular, the snap-back will occur when $\partial\gamma/\partial\phi_{(1)}$ vanishes. By developing this derivative from expression (42), and setting $\phi_{(1)} = 1$, one obtains the following limit condition at the beginning of the postpeak curve:

$$\frac{g_f}{r_0} = 2\left(\frac{1}{\nu^0} + 1\right). \tag{45}$$

For the value of $\nu^0 = 0.2$ used in the example, the condition for no snap-back becomes $g_f/r_0 > 12$, which is in good agreement with Fig. 6(a). Note also that this value would be higher for lower Poisson's ratios and,

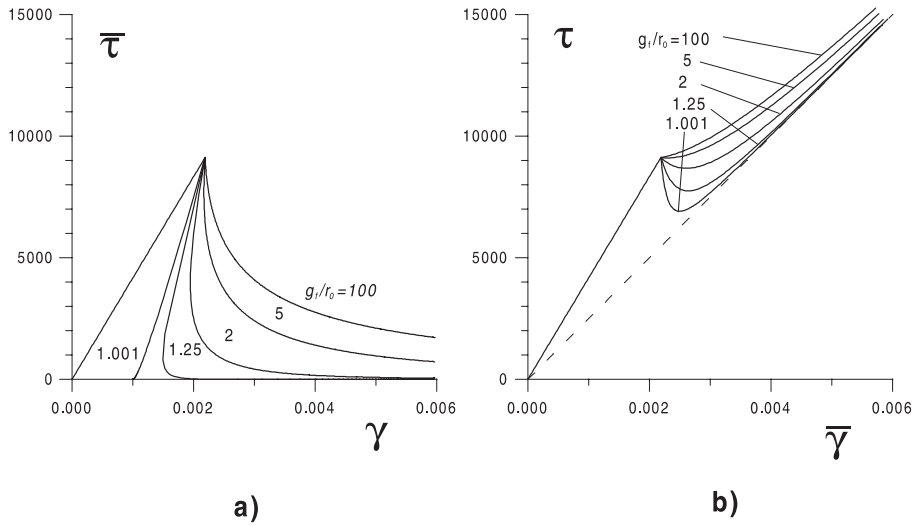

Fig. 6. The results obtained with generalized pseudo-Rankine model with $b > 0$ (anisotropic damage) under (a) pure shear loading, and (b) pure distortion loading, for different values of the parameter g_f.

in the limit case of $v^0 = 0$, would become infinite. In this case, the response would always exhibit snap-back, no matter how large the value used for g_f/r_0.

4.2. Pure distortion for $b > 0$ (anisotropic damage)

In this alternative loading case, principal strains 1 and 2 are prescribed with same intensities $\bar{\gamma}/2 > 0$ and opposite signs, while stress on axis 3 is maintained zero (plane stress). As before, only the first principal component of the inverse integrity tensor $\phi_{(1)}$ grows from its initial unit value, while the other two remain unchanged $\phi_{(2)} = \phi_{(3)} \equiv 1$. This implies the following nominal and effective strains and stresses:

$$\epsilon_{(1)} = \frac{\bar{\gamma}}{2}, \qquad \epsilon_{(2)} = -\frac{\bar{\gamma}}{2}, \tag{46a, b}$$

$$\epsilon^{\text{eff}}_{(1)} = \frac{1}{\phi_{(1)}}\frac{\bar{\gamma}}{2}, \qquad \epsilon^{\text{eff}}_{(2)} = -\frac{\bar{\gamma}}{2}, \tag{47a, b}$$

$$\sigma^{\text{eff}}_{(1)} = G^0\bar{\gamma}\frac{1 - v^0\phi_{(1)}}{(1 - v^0)\phi_{(1)}}, \quad \sigma^{\text{eff}}_{(2)} = -G^0\bar{\gamma}\frac{\phi_{(1)} - v^0}{(1 - v^0)\phi_{(1)}}, \quad \sigma^{\text{eff}}_{(3)} = 0, \tag{48a–c}$$

$$\sigma_{(1)} = G^0\bar{\gamma}\frac{1 - v^0\phi_{(1)}}{(1 - v^0)\phi^2_{(1)}}, \quad \sigma_{(2)} = \sigma^{\text{eff}}_{(2)}, \quad \sigma_{(3)} = 0. \tag{49a–c}$$

From these, one can obtain the out-of-plane strains

$$\epsilon_{(3)} = \epsilon^{\text{eff}}_{(3)} = -\frac{v^0}{1 - v^0}\frac{1 - \phi_{(1)}}{\phi_{(1)}}\frac{\bar{\gamma}}{2}. \tag{50a, b}$$

The identification of the stress quantity τ conjugate to $\bar{\gamma}$, follows a similar procedure as in the case of fixed stress ratio, leading to

$$\tau = \frac{1}{2}(\sigma_{(1)} - \sigma_{(2)}) = \frac{1}{2}G^0\bar{\gamma}\frac{1 - 2v^0\phi_{(1)} + \phi^2_{(1)}}{2(1 - v^0)\phi^2_{(1)}}. \tag{51a, b}$$

In the elastic range, this strain history produces the same results as in the previous section, which can be verified by setting $\phi_{(1)} = 1$ in both sets of equations. Stress and strain at the contact point with the loading surface (onset of damage evolution) are also the same τ_0 and γ_0 given by Eqs. (39) and (43). After peak, enforcement of $F = 0$ with the current value of r leads to the expression of $\bar{\gamma}$ in terms of the damage variable $\phi_{(1)}$:

$$\bar{\gamma} = \gamma_0\sqrt{\frac{1 - v^0}{1 - v^0\phi_{(1)}}}\phi^{1-(r_0/g_f)}_{(1)}. \tag{52}$$

Replacing this expression into previous Eqs. (46a,b)–(51a,b), one obtains all the remaining variables of the problem in terms of $\phi_{(1)}$, and, in particular, that of the conjugate stress:

$$\tau = \tau_0\frac{1 - 2v^0\phi_{(1)} + \phi^2_{(1)}}{2(1 - v^0)}\sqrt{\frac{1 - v^0}{1 - v^0\phi_{(1)}}}\phi^{-1-(r_0/g_f)}_{(1)}. \tag{53}$$

As before, the solutions turn out to be independent of parameter b (degree of anisotropy of the model), as long as $b > 0$. Eqs. (52) and (53) may be used as parametric expressions for $\bar{\gamma}$ and τ in terms of the always-increasing variable $\phi_{(1)} \geqslant 1$. In this way, pairs of values have been obtained and plotted in Fig. 6(b), for the same parameters and values of g_f/r_0 as in previous section.

In Fig. 6(b), it can be seen that this case is considerably more stable than the previous one. Although right after the peak most of the curves exhibit softening, none of them has snap-back. Initial negative slopes rapidly decrease and change sign, and all the curves end up approaching the same asymptote with positive slope (dashed line in the figure). The curve for the highest value of $g_f/r_0 = 100$ skips the softening altogether, starting after the peak directly with hardening. The limit value of g_f/r_0 for this transition may be calculated again with Eq. (44). In this case, $\partial\bar{\gamma}/\partial\phi_{(1)}$ is always positive, and the horizontal tangent corresponds to the zero of $\partial\tau/\partial\phi_{(1)}$. Developing this condition, and setting $\phi_{(1)} = 1$, one obtains

$$\frac{g_f}{r_0} = 2\left(\frac{1}{\nu^0} - 1\right). \tag{54}$$

Using $\nu^0 = 0.2$, this formula leads to $g_f/r_0 = 8$, which is in good agreement with Fig. 6(b). Note also that this limit value is higher for lower Poisson's ratios, becoming $g_f/r_0 = \infty$ for the limit case of $\nu^0 = 0$, i.e. in this case, all the curves would start in the softening regime no matter how large the value of g_f/r_0 is.

Another interesting peculiarity of this case is that even if the prescribed strain is increased unlimitedly $\bar{\gamma} \to \infty$, the damage expressed in terms of the inverse integrity $\phi_{(1)}$ does not grow indefinitely, but it reaches asymptotically a finite value. This value may be obtained from the expression of $\bar{\gamma}$ (52), which becomes infinity as the denominator vanishes. This translates into the condition

$$\phi_{(1)}^{\max} = \frac{1}{\nu^0}. \tag{55}$$

For the value $\nu^0 = 0.2$ used in the example, this yields an asymptotic value of $\phi_{(1)}^{\max} = 5$. The slope of the asymptotic stiffness may also be obtained from previous equations as the ratio $\tau/\bar{\gamma}$ when the limit value $\phi_{(1)} = 5$ is approached. By doing so, one obtains $\tau/\bar{\gamma} = E^0/4 = G_0(1+\nu^0)/2$, which is the slope of the dashed line represented in Fig. 6(b).

The fact that in this loading case, τ always ends up increasing regardless of g_f/r_0, may be interpreted physically because damage is only allowed to develop in the tensile direction, while stiffness in the compressive direction remains unchanged. When damage starts, stress in the tensile direction decreases, more abruptly at the beginning and then progressively more slowly, while in the compressive direction stress always increases. Thinking of a Mohr diagram, the shear stress is given by the radius of the Mohr circle. Initially, the decrease rate of the tensile stress may exceed the increase rate of the compressive stress, causing a decrease in shear stress, but sooner or later the increase of compression will overcome the decrease of tension, and shear stress will start increasing again.

4.3. Pure shear or distortion for $b = 0$ (isotropic damage)

In this case, damage is isotropic and therefore the inverse integrity tensor remains spherical, i.e. all three eigenvalues have the same value $\phi_{(1)} = \phi_{(2)} = \phi_{(3)} = \phi$, with ϕ varying from 1 to ∞ as the damage progresses.

As before, one can consider the two loading cases of pure shear and pure distortion. For $b = 0$, however, both cases turn out to coincide. Here we start with pure shear. The prescribed stresses are again given by Eqs. (33a–c), leading in this case to the following effective stresses, and effective and nominal strains:

$$\sigma_{(1)}^{\text{eff}} = \bar{\tau}\phi, \quad \sigma_{(2)}^{\text{eff}} = -\bar{\tau}\phi, \quad \sigma_{(3)}^{\text{eff}} = 0, \tag{56a–c}$$

$$\epsilon_{(1)}^{\text{eff}} = \frac{\bar{\tau}}{2G^0}\phi, \quad \epsilon_{(2)}^{\text{eff}} = -\frac{\bar{\tau}}{2G^0}\phi, \quad \epsilon_{(3)}^{\text{eff}} = 0, \tag{57a–c}$$

$$\epsilon_{(1)} = \frac{\bar{\tau}}{2G^0}\phi^2, \quad \epsilon_{(2)} = -\frac{\bar{\tau}}{2G^0}\phi^2, \quad \epsilon_{(3)} = 0. \tag{58a–c}$$

One can immediately see that $\epsilon_{(1)}$ and $\epsilon_{(2)}$ have identical values and opposite signs, which means that they could be renamed $\gamma/2$ and $-\gamma/2$, and the full equivalence to the pure distortion case could be immediately established.

The strain γ conjugate to $\bar{\tau}$ is now

$$\gamma = \epsilon_{(1)} - \epsilon_{(2)} = \frac{\bar{\tau}}{G^0}\phi^2. \tag{59a, b}$$

The loading surface $F = 0$ is enforced with the resistance function r given by Eq. (29a,b) and the log damage $L = L_{kk}/3$, which for isotropic damage becomes $L = \ln \phi^2$. Replacing all these into $F = 0$, the expression of the prescribed stress $\bar{\tau}$ in terms of ϕ is obtained, which then can be substituted in previous equations to obtain all the remaining variables in terms of ϕ, and in particular that of the conjugate strain γ. The expressions of interest are

$$\bar{\tau} = \tau_0 \phi^{-1-(r_0/g_f)}, \quad \gamma = \gamma_0 \phi^{1-(r_0/g_f)}, \tag{60a, b}$$

where the stress and strain at the contact point, τ_0 and γ_0, are the same as for $b > 0$, Eqs. (39) and (43).

Parametric equations (60a,b) look simpler than their anisotropic counterparts (41) and (42) or (52) and (53). Actually, in this case, it is possible to isolate ϕ in terms of γ from the second equation and replace in the first. The result is the explicit relation,

$$\bar{\tau} = \tau_0 \left(\frac{\gamma}{\gamma_0} \right)^{-(g_f+r_0)/(g_f-r_0)}, \tag{61}$$

which is valid after damage starts, for $\gamma > \gamma_0$.

The curves defined by Eq. (61) are plotted in Fig. 7, for the same fixed elastic parameters $E^0 = 10^7$ kPa and $v^0 = 0.2$, and the same values of $g_f/r_0 = 1.001$, 1.25, 2, 5 and 100, as in the previous section. In this case, all the curves exhibit similar trends. Although the exponential type of decay is more pronounced for lower g_f/r_0 (and becomes a vertical drop for the limit case $g_f/r_0 = 1$), eventually all the curves approach the horizontal axis, and none of them exhibits snap back. These facts, together with the equivalence between

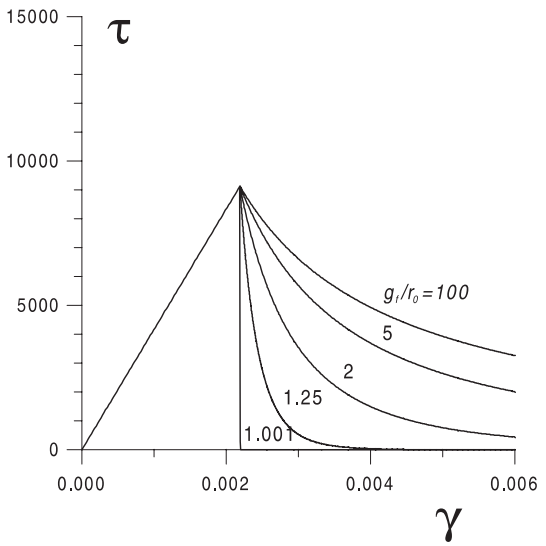

Fig. 7. The results obtained with generalized pseudo-Rankine model with $b = 0$ (isotropic damage) under pure shear/distortion loading, for different values of the parameter g_f.

prescribed shear and prescribed distortion loading, show how the response of the traditional isotropic damage model can deviate substantially (not only quantitatively, but also qualitatively) from that predicted with an anisotropic formulation.

4.4. Dependency of tensile strength on previous tensile loading in perpendicular direction, for $b > 0$

Another analytical solution of practical interest is the influence on the uniaxial stress response, of a previous uniaxial tension loading and unloading in a perpendicular direction. This is only developed for the anisotropic version of the model ($b > 0$), because with isotropic damage the influence is trivial (i.e. the stress–strain diagram in the y-direction continues the unloading–reloading path initiated in the x-direction as if direction had not changed).

To develop this case, we consider a load history with three steps. First, uniaxial loading is applied along the x axis until some post-peak state; second, this stress is unloaded completely; and third, a second uniaxial load is applied along the y axis.

The response to the first uniaxial loading along x is the same as developed in Section 3. Evolution of all variables is given by Eqs. (30a–c)–(32a–c) and represented in Fig. 5. If the maximum strain prescribed during this first part of the load history is $\epsilon_{xx} = \epsilon^* > \epsilon_t$, the values reached by the other evolving variables will be

$$\sigma_{xx} = \sigma^* = \sigma_t \left(\frac{\epsilon^*}{\epsilon_t}\right)^{-(g_f+r_0)/(g_f-r_0)},$$
$$\phi_{xx} = \phi^* = \left(\frac{\epsilon^*}{\epsilon_t}\right)^{g_f/(g_f-r_0)},$$
$$L = L^* = \frac{2}{3}\ln\left(\frac{\epsilon^*}{\epsilon_t}\right)^{g_f/(g_f-r_0)},$$
$$r = r^* = r_0\left(\frac{\epsilon^*}{\epsilon_t}\right)^{-2r_0/(g_f-r_0)}. \tag{62a–d}$$

At the same loading stage, stiffness will have degraded according to the general expression (57) of Part I. In matrix form, the corresponding compliance is

$$\mathbf{C}^* = \frac{1}{E^0}\begin{bmatrix} (\phi^*)^2 & -\phi^* v^0 & -\phi^* v^0 & & & \\ -\phi^* v^0 & 1 & -v^0 & & & \\ -\phi^* v^0 & -v^0 & 1 & & & \\ & & & 2\phi^*(1+v^0) & & \\ & & & & 2(1+v^0) & \\ & & & & & 2\phi^*(1+v^0) \end{bmatrix}. \tag{63}$$

Upon unloading (second part of the load history), stress and strain will go back to zero, while the secant compliance $\mathbf{C}^*$ remains unchanged. ϕ_{xx}, L and r will also keep their modified values $\phi^* > 1$, $L^* > 0$ and $r^* < r_0$.

In the third part of the load history, uniaxial tensile loading is applied along direction y. Until the loading surface is reached again, the material responds elastically according to the secant compliance $\mathbf{C}^*$. However, note that the diagonal component 2,2 in matrix (63) remains unchanged, i.e. the uniaxial compliance along y is still the initial $1/E^0$. Also, the principal integrity value along this axis remains unchanged and equal to 1 (no damage); thus, we can write

$$\sigma_{yy} = \sigma_{yy}^{\text{eff}} = E^0 \epsilon_{yy}, \tag{64}$$

Table 1
Tensile strength reduction $\sigma_{yy}^{\max}/\sigma_t$ due to previous loading in perpendicular direction

σ_{xx}^*/σ_t	0.8	0.6	0.4	0.2	0.1
$\sigma_{yy}^{\max}/\sigma_t$ for $g_f = 3r_0$	0.95	0.88	0.80	0.67	0.56
$\sigma_{yy}^{\max}/\sigma_t$ for $g_f = 7r_0$	0.97	0.94	0.89	0.82	0.75

while all other components of stress, nominal and effective, remain zero.

The strength in the y direction will be given by the new contact point with the loading surface, which may be expressed as

$$F = \frac{1}{2}\sigma_{yy}^{\text{eff}}\epsilon_{yy}^{\text{eff}} - r = \frac{\sigma_{yy}^2}{2E^0} - r^* = 0. \tag{65}$$

As r was reduced from r_0 to r^* during the previous loading, the loading surface has shrunk and the new contact value of σ_{yy} will be indeed lower than the initial tensile strength σ_t. Replacing r^* with its expression and making the appropriate substitutions, one can finally reach the expression:

$$\frac{\sigma_{yy}^{\max}}{\sigma_t} = \left(\frac{\sigma^*}{\sigma_t}\right)^{r_0/(r_0+g_f)} \tag{66}$$

As it is required that $g_f > r_0$ (and most often $g_f > 3r_0$), the exponent on the right-hand side will be smaller than 0.5 (and most often than 0.25), and the fraction $\sigma_{yy}^{\max}/\sigma_t$ will be significantly higher than the fraction σ^*/σ_t. This means that the tensile strength along y, although affected by the previous loading on x, will decrease less (and in general significantly less) than the amount that the strength had been reduced on that axis. This is illustrated with some numerical values for the cases of $g_f/r_0 = 3$ and 7, which are given in Table 1.

It has to be noted again that the previous values (same as all expressions in this section) are only valid for the anisotropic version of the model ($b > 0$). For the isotropic damage model with $b = 0$, the reduction of the strength along y would be identical to the reduction produced during the previous loading along x, i.e. figures in the two horizontal rows in the table would be identical to those in the heading.

On the other hand, one can also try to imagine how the cross-influence on tensile strength could be eliminated altogether. The resistance function assumed in this study $r = r(L)$ is among the simplest possible, and accounts for previous history through the single scalar quantity L. This scalar measure of logarithmic damage can certainly not 'remember' on which direction previous damage was generated, and it is actually remarkable that the effect of some previous damage in a perpendicular direction is somehow reduced, thanks to the interaction with the stiffness, still intact along the loading axis. If desired, complete elimination of the cross-influence on tensile strength should be achieved *via* a more complicated resistance function, which could be made dependent on the whole damage tensor rather than its first invariant, i.e. $r = r(\phi_{ij})$. Such a generalization, however, falls beyond the scope of the present article.

5. Numerical test with rotation of principal directions

In order to investigate the behavior of the proposed anisotropic model under general loading situations where principal directions may rotate, the numerical test proposed by Willam et al. (1987) has been chosen. This test has become widely used to verify and compare constitutive models for cracking and damage (Rots, 1988; Oliver et al., 1990; Feenstra and de Borst, 1992; Carol and Prat, 1995; Guzina et al., 1995; Kroeplin and Weihe, 1997; Meschke et al., 1998).

The test consists of two loading steps: In the first one, a uniaxial tensile stress is applied in the x direction, bringing the material to the onset of softening (i.e. in this case, the peak of the uniaxial stress–strain law). In the second step, increments of the in-plane strain components ϵ_{xx}, ϵ_{yy} and ϵ_{xy} are prescribed in the proportions 1, 1.5, 1, while the out-of-plane degrees of freedom remain with prescribed zero stress. This represents an increment of positive (tensile) strain for both principal directions, accompanied by a rotation of principal axes. The rotation pace is faster at the beginning and progressively slower later on, with a final asymptotic value of 52.02°. The parameter values $E^0 = 10^7$ kPa, $\nu^0 = 0.2$ and $\sigma_t = 10^4$ kPa are the same as in the previous section. Fracture energy is taken as $g_f = 15$ kPa, i.e. three times the elastic energy at peak. The results are presented for values of $b = 0$ (isotropic damage), 0.5, 1, 5 and 40 (close to 'pure' pseudo-Rankine).

In Fig. 8(a), the prescribed strain components ϵ_{yy}, ϵ_{xy} and the resulting principal in-plane strains $\epsilon_{(1)}$ and $\epsilon_{(2)}$, are plotted against the prescribed strain along the x-axis, ϵ_{xx}, which is taken in all subsequent plots as a reference 'time variable'. The angle of rotation of the major principal strain which is implied by previous prescribed values, is plotted in Fig. 8(b). The results obtained with the model in terms of stress, effective stresses, conjugate forces, damage values and rotation of principal directions of all these quantities, are illustrated in Figs. 9–14.

In Fig. 9, the evolution of stress components σ_{xx}, σ_{yy}, σ_{xy} and principal stresses $\sigma_{(1)}$ and $\sigma_{(2)}$, are shown together in four figures for the values of $b = 0$ (isotropic damage), $b = 1$, $b = 5$ and $b = 40$. In Fig. 10, the same set of curves are regrouped into four plots, each representing the evolution of a single stress component obtained for the various values of b. From the figures, it is apparent that, as the parameter b increases and we approach the pseudo-Rankine loading surface, the stress evolution becomes progressively different from the one obtained with isotropic damage. The main differences observed are the inversion of sign of the shear stress, the higher increase of σ_{yy} that at some point overcomes σ_{xx}, the short horizontal plateau in the σ_{xx} stress component towards the middle of its descending branch and, perhaps the most salient, the secondary peak that appears around the middle of the descending curve of the major principal stress.

Unfortunately, in the literature on concrete and quasi-brittle materials, there seems to be no experimental information for this type of tensile test with rotation of principal directions. This is probably due to

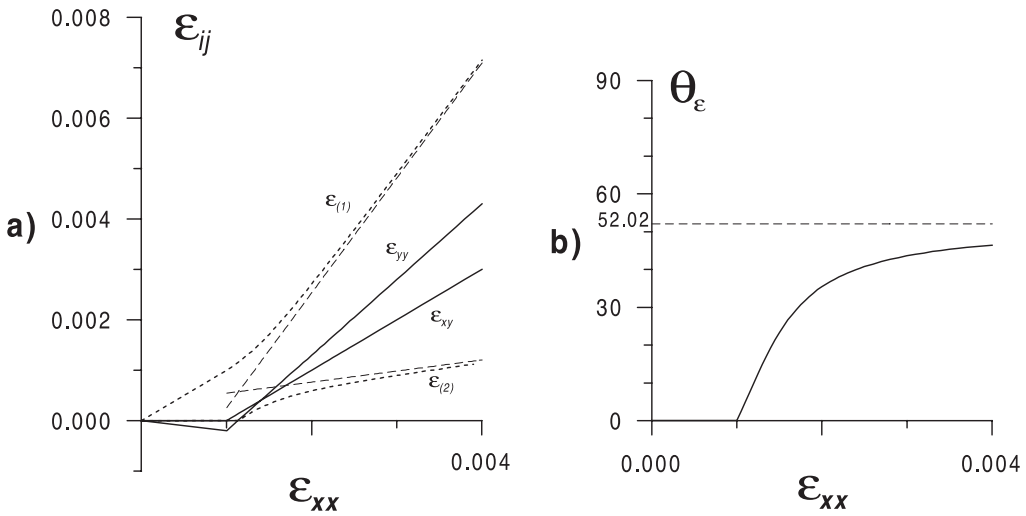

Fig. 8. The prescribed strain for Willam's test. Evolution, with respect to component ϵ_{xx}, of (a) components ϵ_{yy}, ϵ_{xy} and principal values $\epsilon_{(1)}$, $\epsilon_{(2)}$, and (b) angle of major principal direction of strain with x-axis.

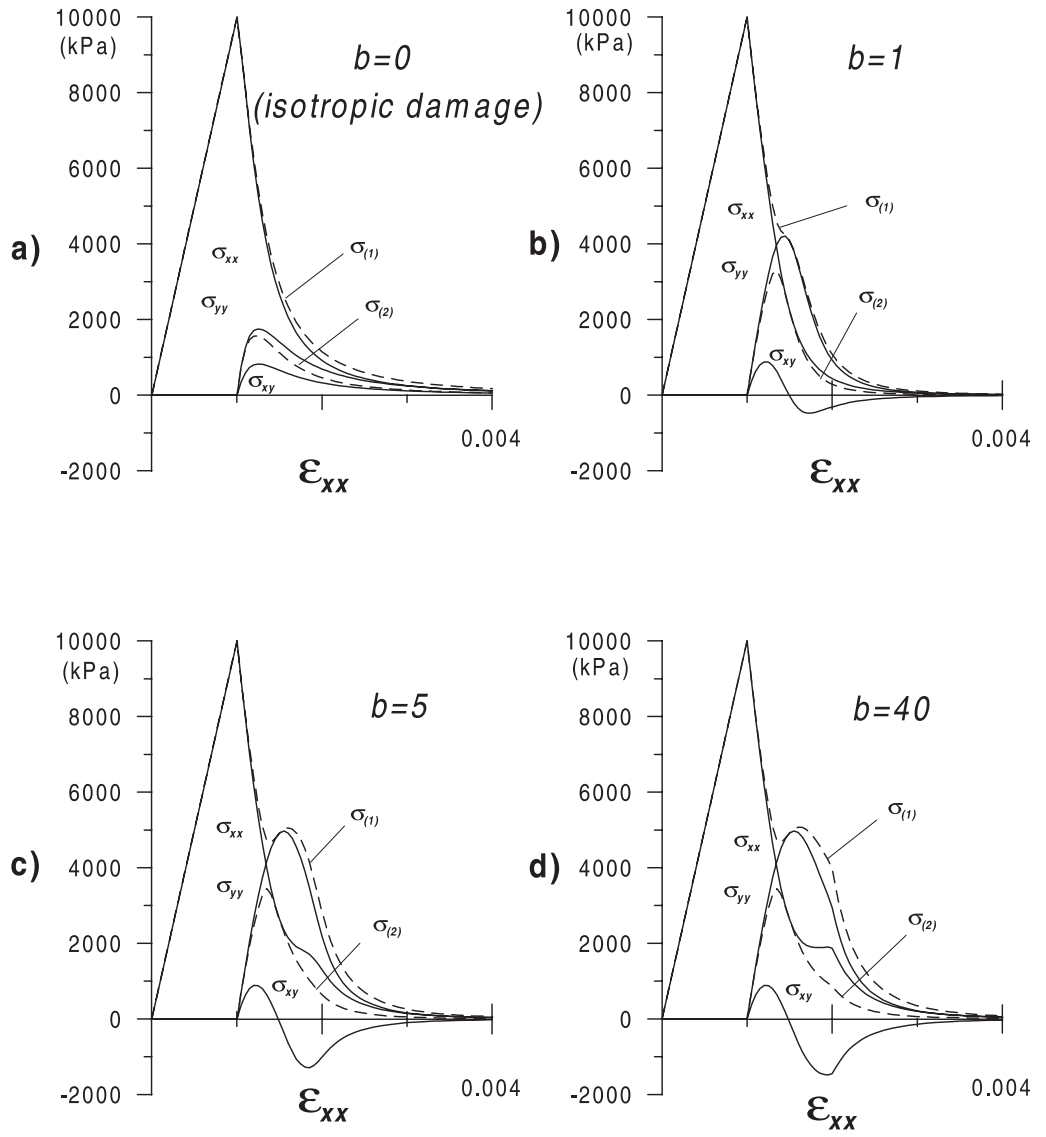

Fig. 9. The results of generalized pseudo-Rankine model subject to Willam's test. The evolution of in-plane stress components and principal values with prescribed strain ϵ_{xx} for (a) $b = 0$, (b) $b = 1$, (c) $b = 5$ and (d) $b = 40$.

the numerous practical difficulties that would be involved in such a laboratory test. Comparison is therefore restricted to other numerical results. Phenomena such as secondary peaks or shear inversion have been previously reported with some smeared cracking or damage models. In general, those were more complicated models with a number of arbitrary parameters such as the crack threshold angle or the shear retention factor (Rots, 1988; Oliver et al., 1990; de Borst et al., 1994; Weihe et al., 1998), models using separate yield surfaces for each of the potential crack planes with its own inelastic multiplier, softening history, etc. (Carol and Prat, 1995; Kroeplin and Weihe, 1997), or multidissipative models combining damage and plasticity (Meschke et al., 1998). It is a pleasant surprise that the proposed generalized pseudo-Rankine model, with

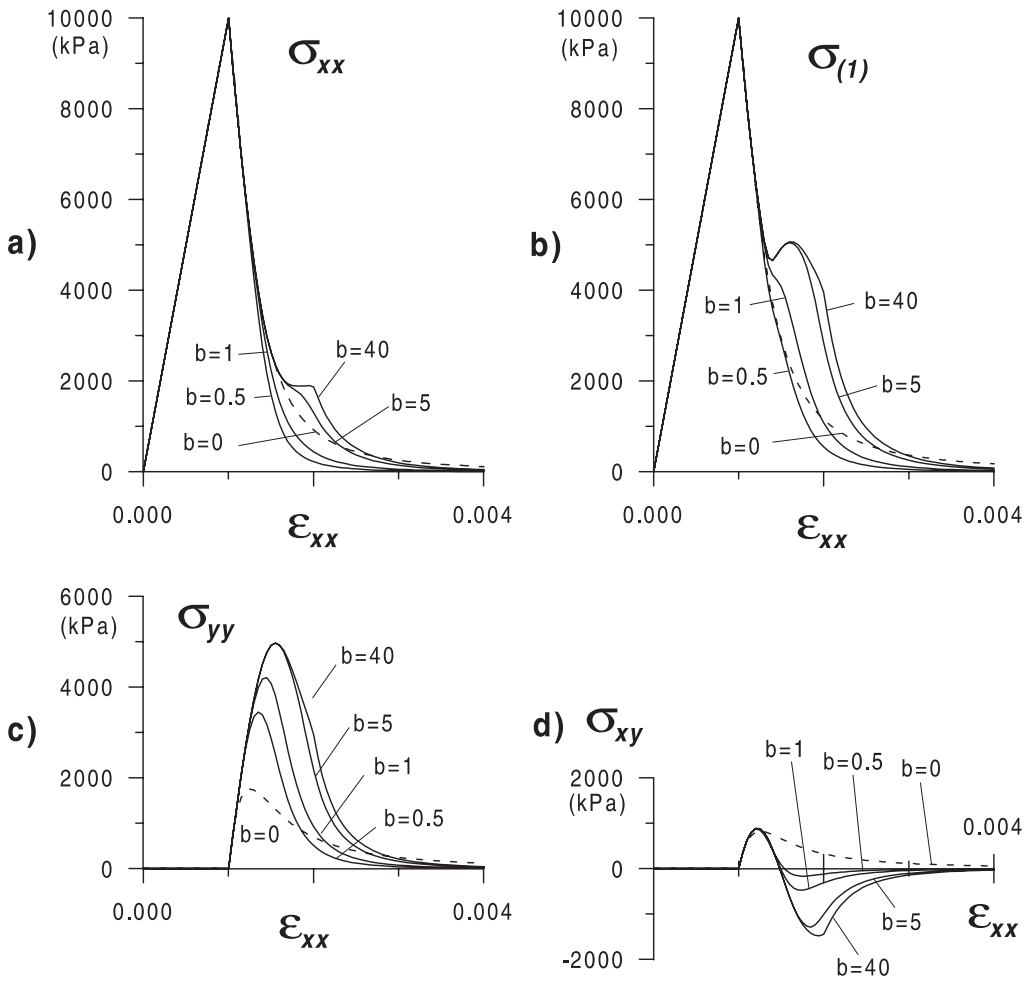

Fig. 10. The results of generalized pseudo-Rankine model subject to Willam's test. The evolution of stresses with respect to prescribed strain ϵ_{xx} and for various values of b: (a) component σ_{xx}, (b) eigenvalue $\sigma_{(1)}$, (c) component σ_{yy}, and (d) component σ_{xy}.

only five parameters and one of the simplest resistance functions possible, is nevertheless capable of representing this type of features.

In Fig. 11, similar illustrations as in Fig. 9 are shown for the effective stresses. Each plot contains the evolution of in-plane components and principal values of the effective stresses, for a fixed value of parameter b that may be 0, 1, 5 or 40. Although different in magnitude, these plots are qualitatively similar to those of the conjugate forces $-\mathscr{Y}_{ij}$, represented in Fig. 12. Very interesting is the fact that, as b is assumed larger and the loading surface closer to pure pseudo-Rankine, at some advanced point of the loading sequence the effective stress tensor becomes spherical, with vanishing shear components and converging values of σ^{eff}_{xx}, σ^{eff}_{yy}, $\sigma^{\text{eff}}_{(1)}$ and $\sigma^{\text{eff}}_{(2)}$. This is specially pronounced in the plot for $b = 40$, and clearly corresponds to the fact that the current point reaches the 'smoothed vertex' of the pseudo-Rankine surface, which is the only region with a normal along the p-axis, i.e. with a damage rule producing increments of purely isotropic degradation. Note that this transition point also coincides with abrupt changes of slope of some of the curves in previous Figs. 10 and 11, particularly with the end of the plateau in the σ_{xx} curve (and similarly in the $\bar{\phi}_{xx}$ curve shown later in Fig. 13). One small but interesting difference in the plots of the conjugate forces

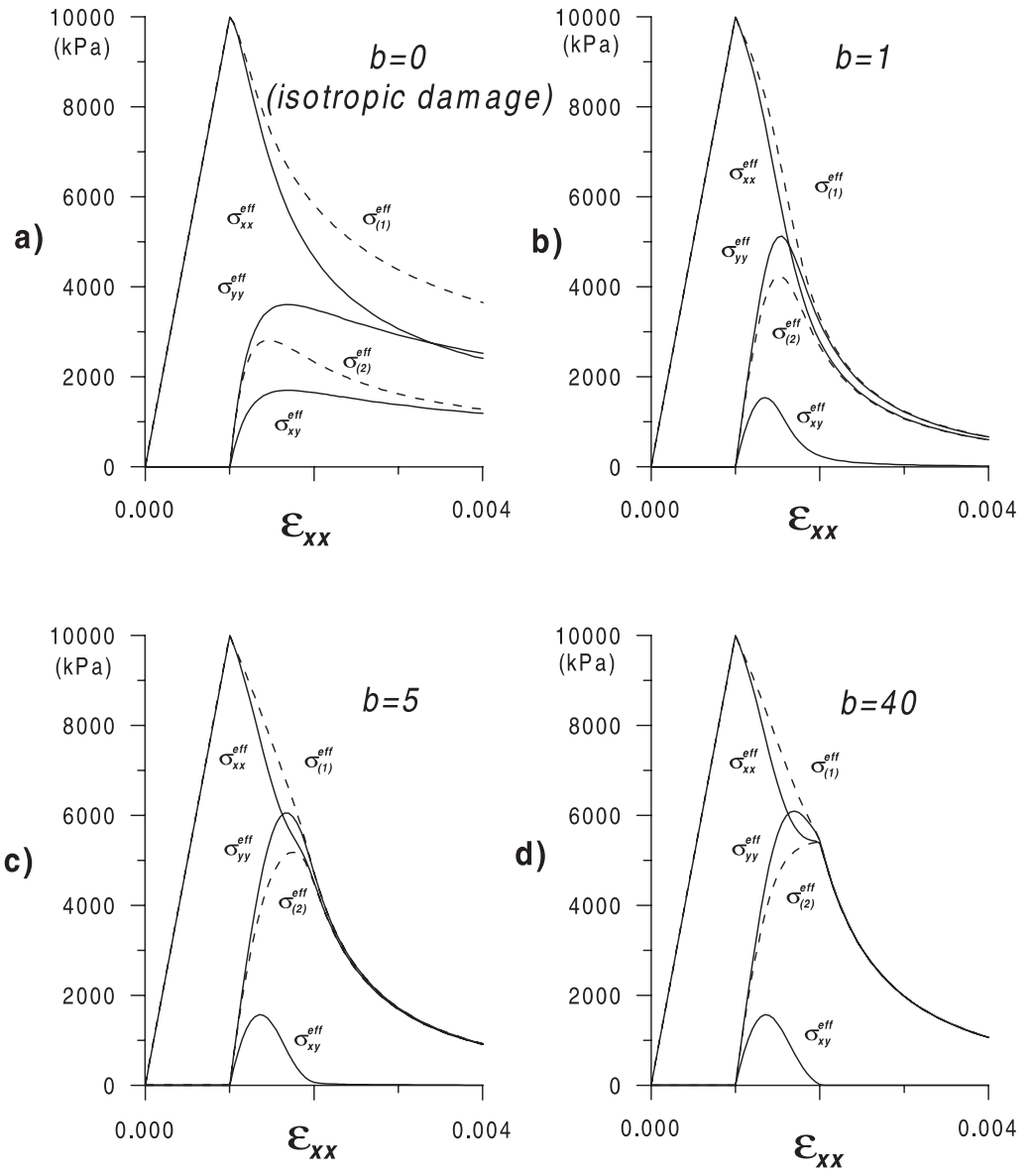

Fig. 11. The results of generalized pseudo-Rankine model subject to Willam's test. The evolution of in-plane effective stress components and principal values with prescribed strain ϵ_{xx} for (a) $b = 0$, (b) $b = 1$, (c) $b = 5$ and (d) $b = 40$.

(Fig. 12) is the slight negative values observed for the $-\mathscr{Y}_{yy}$ and $-\mathscr{Y}_{(2)}$ curves, at the beginning of the second part of the test. In any case, these negative values have no practical consequence given the modified forces defined in Section 2, with which negative values are set to zero.

In Fig. 13, the evolution of the components of the integrity tensor $\bar{\phi}_{ij}$ (inverse to ϕ_{ij}), is presented in four graphs for $b = 0$, $b = 1$, $b = 5$ and $b = 40$. For the integrity tensor, the lowest principal value has been considered as $\bar{\phi}_{(1)}$ because it corresponds to the direction with the largest amount of damage. It can be seen in the figures that, as b is higher, the difference between the principal values 1 and 2 increases, one becoming

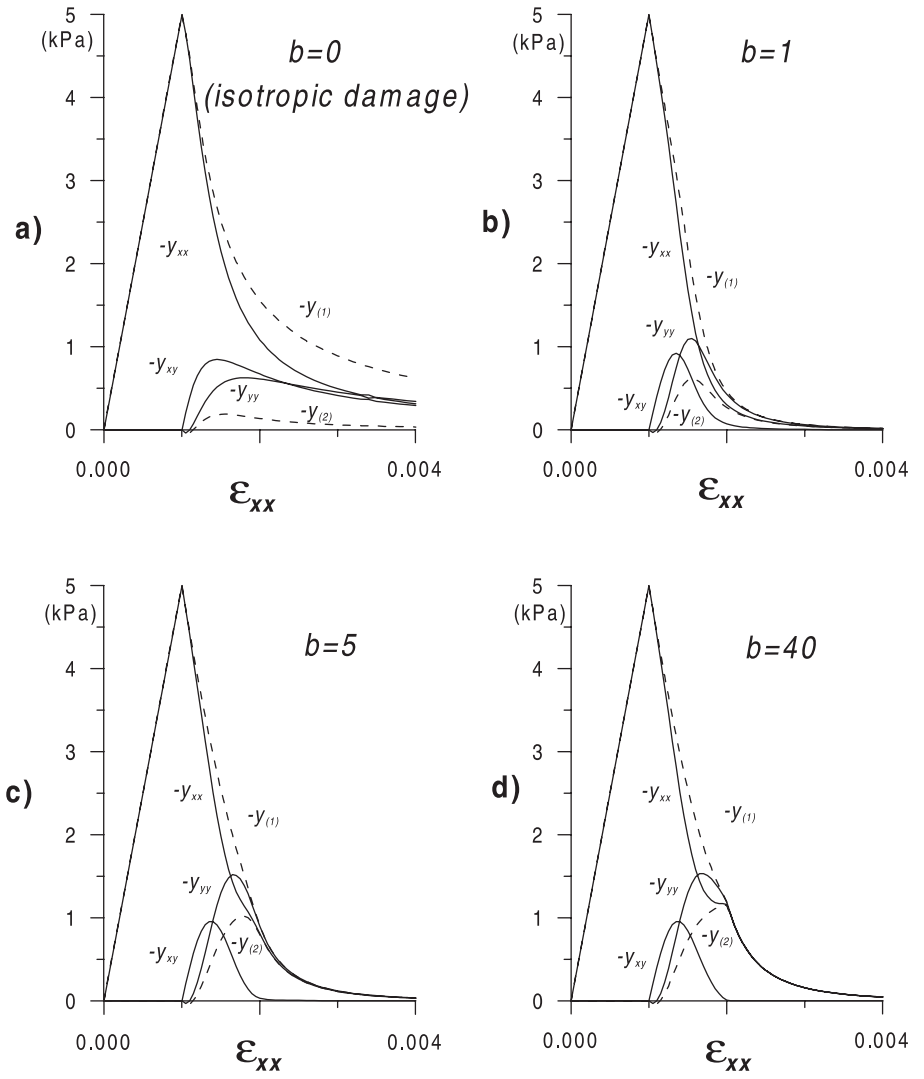

Fig. 12. The results of generalized pseudo-Rankine model subject to Willam's test. The evolution of in-plane conjugate force components and principal values with prescribed strain ϵ_{xx} for (a) $b = 0$, (b) $b = 1$, (c) $b = 5$ and (d) $b = 40$.

considerably larger and the other smaller (by a factor up to 5) than the damage obtained in the isotropic case ($b = 0$). For higher values of b, a small plateau starts to appear in the descending curve of $\bar{\phi}_{xx}$, around the value 0.4. This plateau, which ends abruptly when ϵ_{xx} equals about twice the peak strain, coincides very well with the one observed for nominal stresses.

In Fig. 14, the evolution of the angles of the major principal directions is depicted in four plots. The first of them represents the evolution of the orientation of the major principal directions of stresses, effective quantities and damage for $b = 1$, together with the (prescribed) orientation of the major principal strain. In each of the second, third and fourth plots, the evolution of one of those orientations is depicted for the various values of b. In the case of isotropic damage ($b = 0$), coaxiality is maintained, and therefore curves for stress or effective stress coincide with the curve for the angle of prescribed strain, which is included in all plots (for damage it does not make sense to talk about principal direction in this case, as the tensor remains

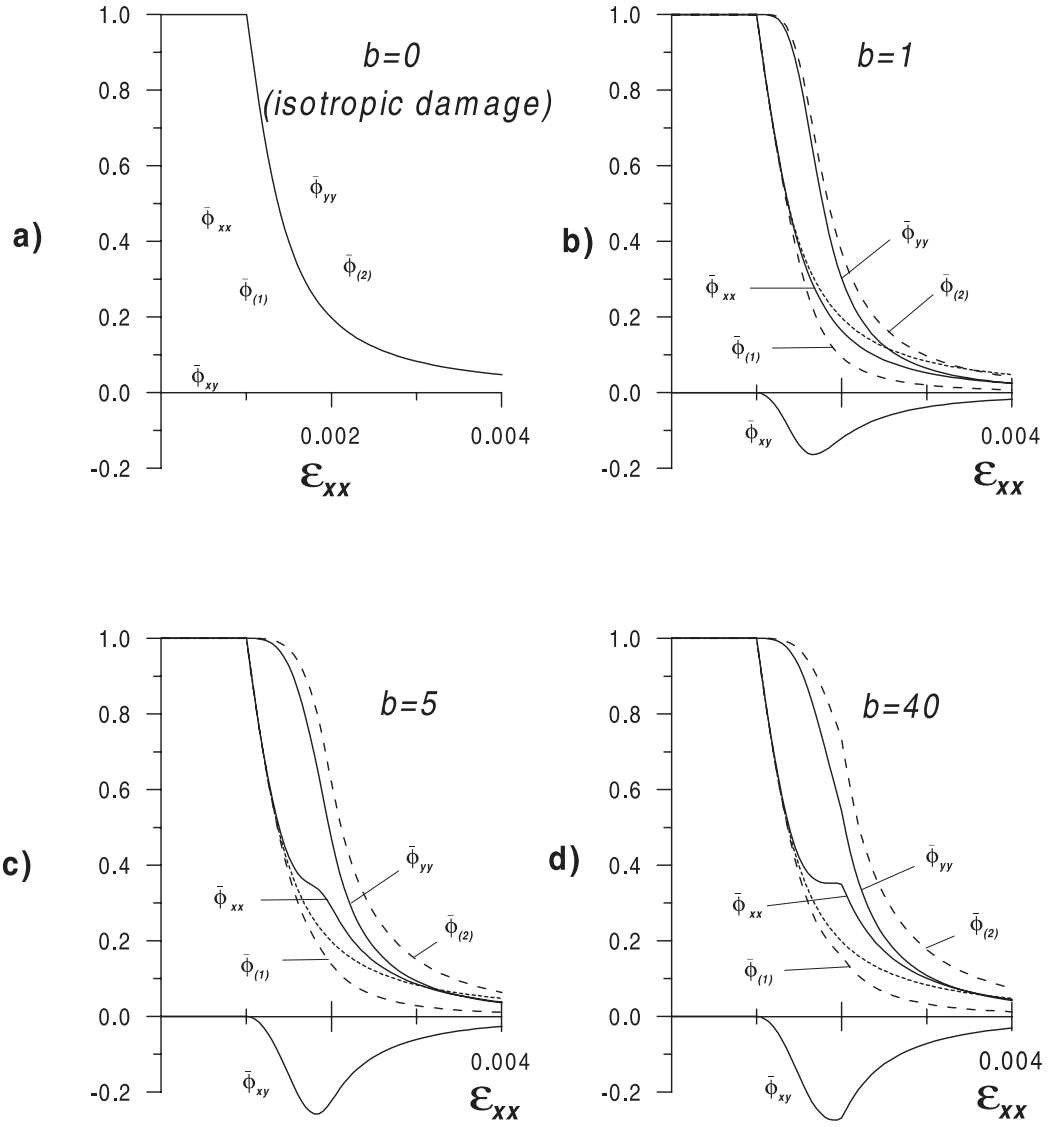

Fig. 13. The results of generalized pseudo-Rankine model subject to Willam's test. The evolution of in-plane damage components $\bar{\phi}_{xx}$, $\bar{\phi}_{yy}$ and principal values $\bar{\phi}_{(1)}$ and $\bar{\phi}_{(2)}$ with prescribed strain ϵ_{xx}, for (a) $b = 0$, (b) $b = 1$, (c) $b = 5$ and (d) $b = 40$.

isotropic). Examining all different response features, we note the general tendency that the rotation of damage falls slightly behind the rotation of the driving strain, while both effective stress, and especially nominal stress, significantly overtake the prescribed strain rotation. This may be explained with the argument that damage weakens the material in directions of previous principal strain, and under application of a subsequent increment of strain, the corresponding increments of stress overrotate, following the general principle that the stiffer part always takes more stresses. For $b = 40$, it is apparent that as the smooth corner of the pseudo-Rankine surface is reached and degradation increments become fully isotropic, the damage also becomes coaxial with prescribed strain. At the same time, effective stresses stop rotating (actually the rotation is slightly reversed) and the rotation rate of stresses is drastically reduced.

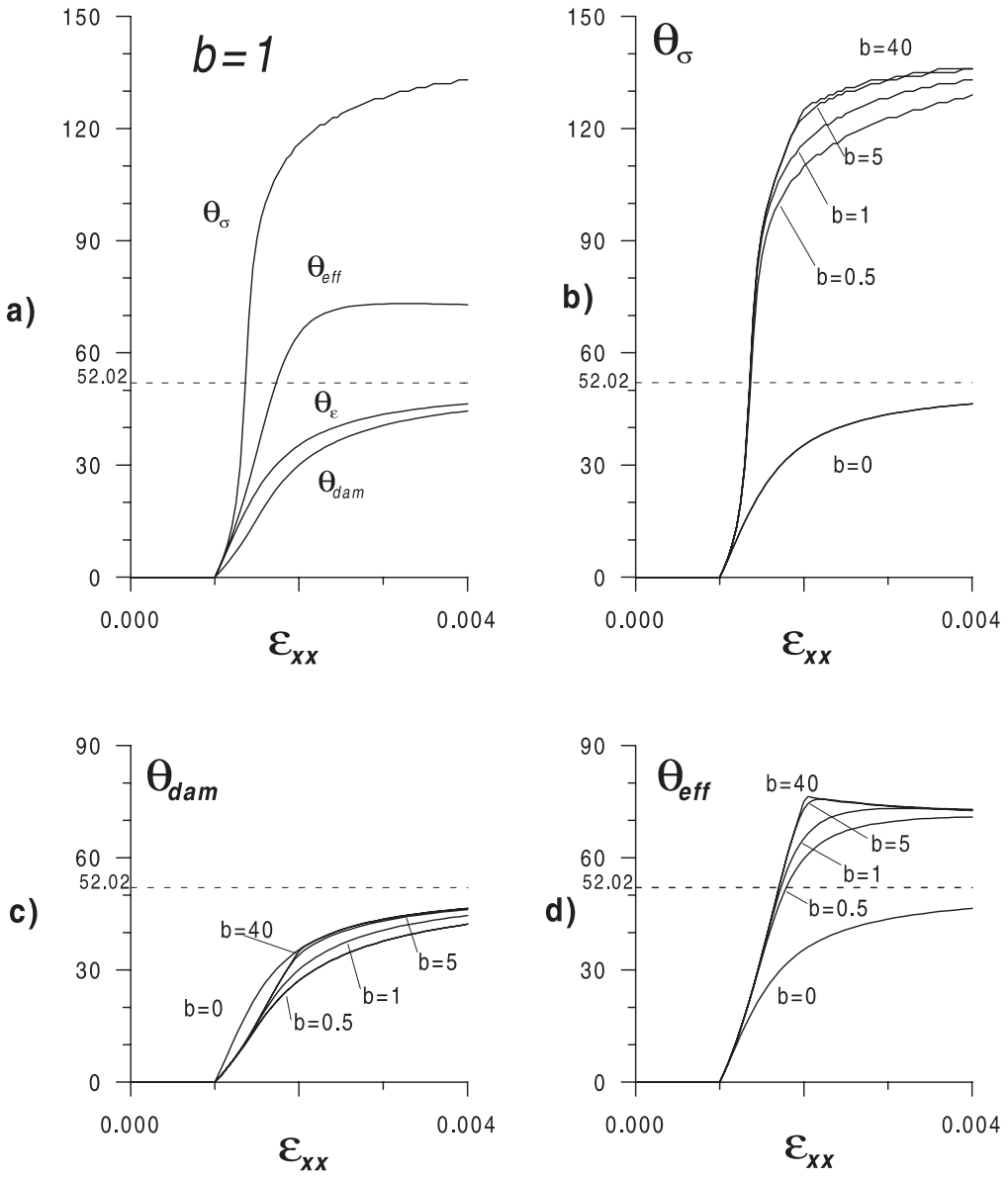

Fig. 14. The results of generalized pseudo-Rankine model subject to Willam's test. The evolution of angles between x-axis and major principal directions of (a) stress, damage, effective stress and strain for $b = 0$, (b) stress for various values of b, (c) damage for various values of b, and (d) effective stress for various values of b.

6. Concluding remarks

The new concept of pseudo-logarithmic rate of damage was introduced in 'Part I'. This damage rate and the corresponding conjugate forces exhibit convenient properties, which greatly simplify the task of defining loading surface and evolution laws for anisotropic damage.

In this 'Part II', a specific model is developed within the new framework. First, modified conjugate forces are defined, which make it possible to distinguish tension and compression cases and avoid negative dissipation. The loading surface is then defined in the space of these modified forces. Depending on a single parameter b, a family of shapes is generated between the π-plane (classical isotropic damage) and the Rankine-type surface (maximum anisotropic damage). Equipped with very simple evolution laws, the model exhibits a closed-form solution in uniaxial tension, which allows us to identify the damage parameters in terms of physical quantities that can be measured in the laboratory such as σ_t and g_f. Together with E^0, ν^0 and b, this makes a total of only five material parameters for the anisotropic damage model. The fact that g_f is one of the parameters, is also very convenient for implementing energy regularization procedures at the finite element level.

Additional closed-form solutions are presented for pure shear and pure distortion, as well as the influence on the tensile strength, of a previous loading/unloading sequence in a perpendicular direction. These solutions clearly show how the response of the isotropic damage model ($b = 0$) may differ substantially from that of a full anisotropic model ($b > 0$).

In spite of its relative simplicity, this model is capable of representing complex anisotropic response, as obtained from its application to a numerical test in tension/shear with significant rotation of principal strain directions. In these calculations, the generalized pseudo-Rankine model exhibits secondary peaks, and a number of other phenomena only observed so far with more complicated models.

Acknowledgements

Partial support from DGICYT (Madrid, Spain) under research grants PB95-0771 and PB96–0500 is gratefully acknowledged. The second author would like to acknowledge financial support from the Italian Ministry (MURST). The last author also wishes to thank for the partial support from US-NSF through grant CMS–9634923 to the University of Colorado at Boulder. At the initial stages of this study, travel between UPC and the University of Colorado was funded through NATO collaborative research grant no. CRG.961177, and grant no. GRQ93–3012 from CUR (Generalitat de Catalunya, Barcelona, Spain). A travel grant received from the US-Spain Commission for Educational and Scientific Exchange in 1999 is also gratefully acknowledged.

References

Carol, I., Prat, P.C., 1995. A multicrack model based on the theory of multisurface plasticity and two fracture energies. In: Owen, D.R.J., Oñate, E., Hinton, E. (Eds.), Computational Plasticity (COMPLAS IV), vol. 2, Pineridge, Barcelona, pp. 1583–1594.

Carol, I., Rizzi, E., Willam, K., 1994. A unified theory of elastic degradation and damage based on a loading surface. Int. J. Solids Struct. 31 (20), 2835–2865.

Carol, I., Rizzi, E., Willam, K., 2000. On the formulation of anisotropic elastic degradation. part I: theory based on a pseudo-logarithmic damage tensor rate. Int. J. Solids Struct. 38 (4), 491–518.

Chaboche, J.L., Lesne, P.M., Maire, J.F., 1994. Phenomenological damage mechanics of brittle materials with description of the unilateral effects. In: Bažant, Z.P., Bittnar, Z., Jirásek, M., Mazars, J. (Eds.), Fracture and Damage in Quasi-Brittle Structures, E & FN SPON, London, pp. 75–84.

de Borst, R., Feenstra, P., Pamin, J., Sluys, L.J., 1994. Some current issues in computational mechanics of concrete. In: Mang, H., Bićanić, N., de Borst, R. (Eds.), Computational Modelling of Concrete Structures, Pineridge, Innsbruck, pp. 283–302.

Feenstra, P.H., de Borst, R., 1992. The Rankine-plasticity model for concrete cracking. In: Owen, D.R.J., Oñate, E., Hinton, E. (Eds.), Computational Plasticity (COMPLAS III), vol. 1, Pineridge, Barcelona, pp. 657–668.

Guzina, B., Rizzi, E., Willam, K., Pak, R.Y.S., 1995. Failure prediction of smeared crack formulations. ASCE J. Engng. Mech. 121 (1), 150–161.

Kroeplin, B., Weihe, S., 1997. Constitutive and geometrical aspects of fracture-induced anisotropy. In: Owen, D.R.J., Oñate, E., Hinton, E. (Eds.), Computational Plasticity (COMPLAS V), vol. 1, Pineridge, Barcelona, pp. 255–279.

Kupfer, H., Gerstle, K., 1973. Behavior of concrete under biaxial stresses. ASCE J. Engng. Mech. Div. 99, 853–866.

Meschke, G., Macht, J., Lackner, R., 1998. A damage-plasticity model for concrete accounting for fracture-induced anisotropy. In: Mang, H., Bićanić, N., de Borst, R. (Eds.), Computational Modelling of Concrete Structures, Balkema, Badgastein (Austria), pp. 3–12.

Oliver, J., Cervera, M., Oller, S., Lubliner, J., 1990. Isotropic damage models and smeared crack analysis of concrete. In: Bićanić, N., Mang, H. (Eds.), Computer-Aided Analysis and Design of Concrete Structures, vol. 2, Pineridge, Zell-am-See, Austria, pp. 945–957.

Rots, J.G., 1988. Computational modelling of concrete fracture. Ph.D. Thesis, Delft University of Technology, The Netherlands.

Weihe, S., Kroeplin, B., de Borst, R., 1998. Classification of smeared crack models based on material and structural properties. Int. J. Solids Struct. 35 (12), 1289–1308.

Willam, K., Pramono, E., Sture, S., 1987. Fundamental issues of smeared crack models. In: Shah, S.P., Swartz, S.E. (Eds.), SEM-RILEM Int. Conf. on Fracture of Concrete and Rock, Bethel, Connecticut. Society of Engineering Mechanics, pp. 192–207.